

RESEARCH ARTICLE

Proprotein convertase furina is required for heart development in zebrafish

Qinchao Zhou¹, Lei Lei¹, Hefei Zhang², Shih-Ching Chiu¹, Lu Gao¹, Ran Yang¹, Wensheng Wei³, Gang Peng², Xiaojun Zhu^{1,*} and Jing-Wei Xiong^{1,*}

ABSTRACT

Cardiac looping and trabeculation are key processes during cardiac chamber maturation. However, the underlying mechanisms remain incompletely understood. Here, we report the isolation, cloning and characterization of the proprotein convertase *furina* from the cardiovascular mutant *loft* in zebrafish. *loft* is an ethylnitrosourea-induced mutant and has evident defects in the cardiac outflow tract, heart looping and trabeculation, the craniofacial region and pharyngeal arch arteries. Positional cloning revealed that *furina* mRNA was barely detectable in *loft* mutants, and *loft* failed to complement the TALEN-induced *furina* mutant *pku338*, confirming that *furina* is responsible for the *loft* mutant phenotypes. Mechanistic studies demonstrated that Notch reporter *Tg(tp1:mCherry)* signals were largely eliminated in mutant hearts, and overexpression of the Notch intracellular domain partially rescued the mutant phenotypes, probably due to the lack of Furina-mediated cleavage processing of Notch1b proteins, the only Notch receptor expressed in the heart. Together, our data suggest a potential post-translational modification of Notch1b proteins via the proprotein convertase Furina in the heart, and unveil the function of the Furina-Notch1b axis in cardiac looping and trabeculation in zebrafish, and possibly in other organisms.

KEY WORDS: *Furina*, *Loft* mutant, Heart looping, Cardiac trabeculation, Zebrafish

INTRODUCTION

Congenital heart disease is one of the major birth defects in humans. As an asymmetric organ, generation of a functional human heart consists of complex interactions among cardiac cell proliferation, differentiation, maturation and migration coordinated in a spatiotemporal manner. Because of its fecundity, transparency, rapid embryonic development and relatively conserved organogenesis, the zebrafish is a well-recognized model organism in which to unravel the mechanisms underlying the development of organs, such as the heart (Staudt and Stainier, 2012). The knowledge gained from the zebrafish system may help to shed light

on our understanding of the genetic basis of heart diseases, particularly congenital heart diseases.


Cardiac left-right asymmetry starts at early somite stages with the first appearance of a left-sided heart tube. Several signals, such as Nodal, Lefty, Pitx2 and BMP, have been reported to play critical roles in heart tube jogging (Bakkers et al., 2009; Evans et al., 2010). The left-sided tube then undergoes looping, accompanied by the formation of a right-sided ventricle and a left-sided atrium separated by the atrioventricular canal (AVC). Cardiac jogging is a good predictor of subsequent cardiac looping, as jogging defects often lead to an unlooped heart (Bakkers et al., 2009). Although looping is affected by early left-right asymmetry, the seamless formation of a looped heart requires a complex network of molecular signals and interactions of cells from the endocardium, myocardium, second heart field and cardiac neural crests during early organogenesis (Kelly et al., 2014; Lin and Xu, 2009).

Cardiac trabeculation begins at the end of heart looping, when the outer curvature of the ventricle forms a specialized protruding myocardium (Staudt et al., 2014; Wagner and Siddiqui, 2007; Wu, 2018). Trabeculation is essential for normal cardiac function, in which sponge-like muscular structures are generated by precise cardiomyocyte delamination/protrusion, myocardial proliferation and endocardial-myocardial interaction. In zebrafish, three-dimensional time-lapse imaging has revealed that initial trabeculation consists of two major steps, in which cardiomyocytes extend protrusions by invading lumenally along neighbouring cell-cell interactions; and protrusion-forming cardiomyocytes move their somata into the trabecular layer via constricting the abluminal surface (Cherian et al., 2016; Jimenez-Amilburu et al., 2016; Staudt et al., 2014). In mice, cardiomyocytes in the monolayer myocardium display polarity, with oriented cell division and directional migration, which are required for trabecular initiation and formation (Wu, 2018). Several signalling pathways, including Nrg1-ErbB2/4 and Notch1-Hey2, and blood flow/cardiac contractility are essential for cardiac trabecular development and maturation (Luxan et al., 2016).

The Notch signalling pathway is highly conserved in regulating the determination of cell fate through ligand-receptor interactions. Notch receptor activation is involved in three consecutive proteolyses. During their maturation in the Golgi network, Notch precursors are first cleaved by a Furin-like convertase at the S1 site to generate a heterodimeric receptor that interacts with ligands in adjacent cells. When binding with ligands, Notch receptors are cleaved by ADAM metalloprotease at the S2 site. Following S2 cleavage, Notch receptors are cleaved by γ -secretase at the S3 site to release an activated fragment, Notch intracellular domain (NICD; van Tetering and Vooijs, 2011). Notch signalling plays essential roles in cardiac morphogenesis. Mutations of components in the Notch signalling pathway cause both congenital and acquired heart diseases in humans. The functions of Notch signalling in cardiac development and disease are well illuminated in several excellent

¹Beijing Key Laboratory of Cardiometabolic Molecular Medicine, Institute of Molecular Medicine, College of Future Technology, and State Key Laboratory of Natural and Biomimetic Drugs, Peking University, Beijing 100871, China. ²Institutes of Brain Science, State Key Laboratory of Medical Neurobiology and Collaborative Innovation Center for Brain Science, Fudan University, Shanghai 200032, China. ³School of Life Sciences, Peking University, Beijing 100871, China.

*Authors for correspondence (jingwei_xiong@pku.edu.cn; zhuxiaojun@pku.edu.cn)

 J.-W.X., 0000-0001-8438-4782

Handling Editor: Caroline Hill
Received 23 January 2021; Accepted 27 September 2021

reviews (de la Pompa and Epstein, 2012; Luxan et al., 2016; Pedrazzini, 2007).

Furin, a member of the proprotein convertase family, is necessary for the processing of a wide range of proproteins, including growth factors, cell adhesion proteins and receptors. The Furin cleavage site consists of four core recognition amino acids, R-X-(R/K)-R (Seidah, 2011). Inactivation of *Furin* in mice leads to premature death at embryonic day (E)11, with severe failure in cardiac ventral closure and looping morphogenesis (Constam and Robertson, 2000; Roebroek et al., 1998). Conditional deletion of *Furin* in mouse endothelial cells leads to ventricular septal defects and valve malformations, demonstrating an essential role of Furin in endocardial–myocardial interactions and morphogenesis (Kim et al., 2012). Two Furin paralogues, *furina* and *furinb*, have been reported in zebrafish. *Furina* mutation or knockdown of *furina* and *furinb* leads to craniofacial defects via affecting endothelin-1 signalling (Walker et al., 2006). A second *furina* mutant displays defects in left-right asymmetry and heart looping, and the cleavage processing of Spaw proteins by Furin regulates Nodal signalling for the development of cardiac asymmetry (Tessadori et al., 2015). Nevertheless, it remains to be addressed whether the cardiac looping defect is the only consequence of early left-right asymmetric alteration or intrinsic cardiac signalling, or both of these processes. Here, we report the cloning and functional analysis of *furina* in cardiovascular development using the N-ethyl-N-nitrosourea (ENU)-induced *loft* mutant in zebrafish, and thus present an additional layer of regulation of Notch signalling in the heart, probably through the Furina-mediated cleavage of Notch1b proteins, and reveal the critical function of the Furina-Notch1b axis in heart looping and cardiac trabeculation.

RESULTS

Isolation of the ENU-induced heart mutant *loft* in zebrafish

To address the fundamental mechanisms underlying cardiac development and maturation, we isolated the *loft* mutant using unbiased ENU-induced mutagenesis of the AB zebrafish genome as described previously (Shah et al., 2012). During the first 2 days of development, the *loft* mutant developed normally and was

indistinguishable from its siblings. However, *loft* mutants exhibited an open-mouthed jaw, a highly intumescent outflow tract, abnormal heart looping (Fig. 1A,A') and plicated tail fins at 3 days post-fertilization (dpf) (Fig. S1A,B), but the blood circulation of mutants was not affected during the first week of development (Movie 1). The vascular endothelial cell reporter *Tg(kdr1:GFP)* revealed that pharyngeal arch arteries (paa) were formed but new artery budding was affected in the *loft* mutants at 3 dpf (Fig. 1B,B'). As for the intumescent outflow tract of mutants, we applied diaminofluorescein diacetate (DAF-2 DA) staining to measure the accumulated nitric oxide in smooth muscle cells, which revealed much weaker staining in *loft* mutants, suggesting a potential differentiation defect in smooth muscles (Fig. 1C,C'). In addition, the cardiomyocyte progenitor reporter *Tg(nkx2.5:zsYellow)* revealed abnormal cardiac looping at 3 dpf (Fig. 1D') and failure of cardiac trabeculation at 4 dpf in *loft* mutants (Fig. 1E') compared with siblings (Fig. 1D,E). These data show that *loft* mutants have several developmental defects in the heart, jaw, paa and tail fins.

furina is disrupted in *loft* mutants

The cardiac defects encouraged us to pursue positional cloning of the affected gene in the *loft* mutants. By using *loft* AB/WIK mapping zebrafish, we performed genome-wide genetic linkage analysis and mapped it to chromosome 7 using a panel of simple sequence length polymorphism markers. Further fine genetic mapping narrowed its location to between the genetic markers AF-10 and *furina-7* (Fig. 2A), where two RefSeq genes, *slc39a1* and *furina*, were identified. In particular, the genetic marker *furina-7* picked up a single recombination out of 3860 meioses, suggesting that *furina* is a candidate gene for this locus. Nevertheless, extensive sequencing of exons in these two candidate genes failed to identify any informative mutations. To test whether their expression was affected in *loft* mutants, we performed whole-mount RNA *in situ* hybridization with either anti-sense *slc39a1* or *furina* probes. Intriguingly, although *slc39a1* mRNA expression was not affected, *furina* mRNA was barely detectable in *loft* mutants compared with siblings at 48 h post-fertilization (hpf) (Fig. 2B; Fig. S1C,D).

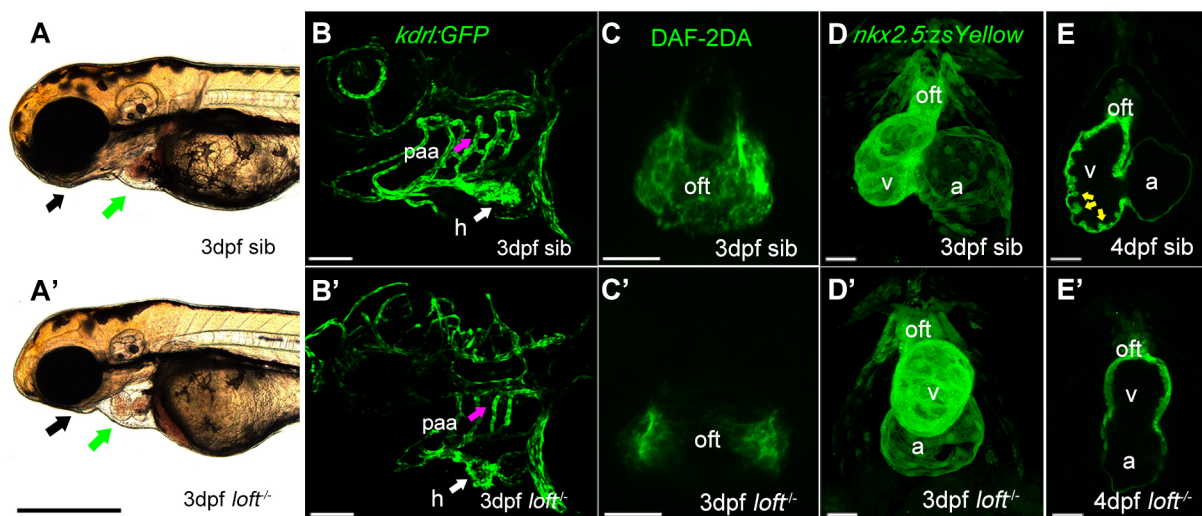


Fig. 1. Jaw and cardiovascular defects are evident in *loft* mutants. (A,A') Bright-field image showing an abnormal open-mouthed jaw (black arrows) and cardiac looping (green arrows) in *loft* mutants (A'), unlike siblings, at 3 dpf (A). (B-E') Lack of paa budding labelled by *Tg(kdr1:GFP)* (B'; magenta arrow), decreased nitric oxide of the outflow tract by DAF-2 DA staining (C'), abnormal cardiac looping labelled by *Tg(nkx2.5:zsYellow)* (D') at 3 dpf, and no ventricular trabeculation labelled by *Tg(nkx2.5:zsYellow)* at 4 dpf (E') in *loft* mutants compared with siblings (B-E). Magenta arrows indicate paa budding (B,B'), white arrows indicate the heart (B,B') and yellow arrows indicate ventricular trabeculation (E). a, atrium; h, heart; oft, outflow tract; v, ventricle. Scale bars: 400 μ m (A,A'); 100 μ m (B,B'); 20 μ m (C,C'); 30 μ m (D-E').

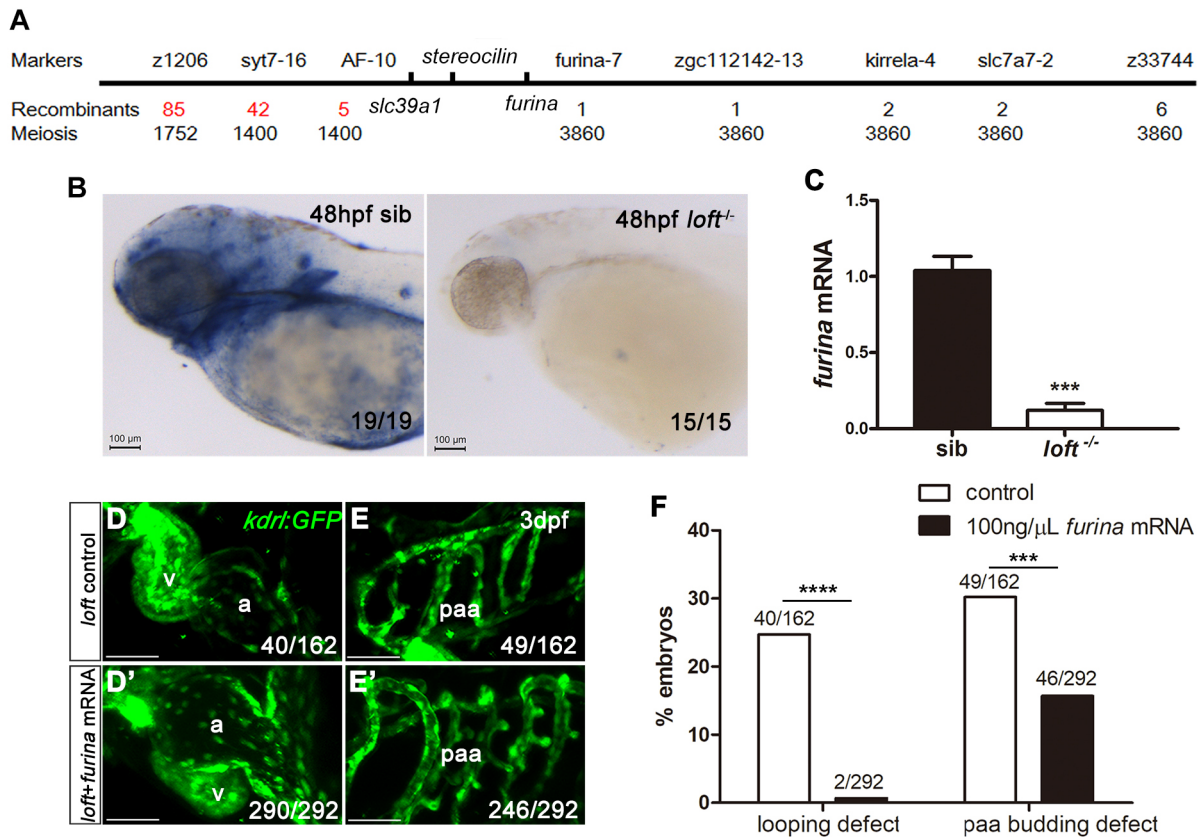


Fig. 2. The *furina* gene is responsible for *loft* mutant defects. (A) Using *loft* (AB/WIK) mapping zebrafish, positional cloning revealed that the *loft* mutation was located between genetic markers AF-10 and *furina-7*. (B) Whole-mount *in situ* hybridization showed that *furina* mRNA expression was barely detected in *loft* mutants (15/15) compared with siblings (19/19) at 48 hpf. (C) qRT-PCR analysis showed that *furina* mRNA expression declined significantly in *loft* mutants compared with siblings at 48 hpf. GAPDH was used to normalize mRNA. (D-E') Embryos from heterozygous *loft* crosses were injected with water (D,E) or 100 ng/μl *furina* mRNA (D',E'). Microinjection of *furina* mRNA rescued almost all the embryos with heart looping defects (290/292) (D), with ~25% percent of the control embryos exhibiting looping defects (40/162) (D'), and partially rescued paa budding defects (246/292) (E), with more than 25% of the control embryos exhibiting budding defects (49/162) (E'). *Tg(kdr:EGFP)* was used to label blood vessels and the endocardium. (F) Statistics show that microinjection of *furina* mRNA suppressed defects in both cardiac looping and paa budding of embryos from heterozygous *loft* crosses. Data are mean±s.d. *** $P < 0.001$, **** $P < 0.0001$ [unpaired two-tailed Student's *t*-test (C, $n=3$); χ^2 test (F)]. a, atrium; v, ventricle. Scale bars: 100 μm (B); 50 μm (D-E').

RT-PCR and RNA-seq data further confirmed the complete loss of *furina* mRNA expression in the mutants, and the expression level of *furinb* was not compensatory upregulated (Fig. 2C; Table S1). To establish the functional relationship of the *furina* gene with the *loft* mutant, we microinjected capped *furina* mRNA into embryos from heterozygous *loft* mutant crosses. Compared with ~25% (40/162) abnormal heart looping (Fig. 2D), a lack of paa budding (49/162) (Fig. 2E) and open-mouthed jaw (54/206) (Fig. S2B) in water-injected embryos, we found ~0.7% (2/292) with abnormal heart looping (Fig. 2D',F), ~15.8% (46/292) (Fig. 2E',F) with a lack of paa budding and ~25.9% (55/212) with a partially rescued jaw (Fig. S2D,E) in *furina*-injected embryos, suggesting that overexpression of *furina* enabled the rescue the mutant phenotypes. Furthermore, microinjection of the *furina* ATG morpholino (0.5 mM) into wild-type embryos resulted in defects in heart looping and paa budding similar to those in *loft* mutants (Fig. S3A,A',E). Although microinjection of the low-dose *furina* morpholino (0.25 mM) into wild-type embryos induced a low percentage of *loft* mutant phenotypes, this morpholino sensitized heterozygous *loft* mutants to generate a high percentage of mutant phenotypes (Fig. S3B-C',E). In contrast, wild-type embryos and heterozygous *loft* mutants had no evident heart defects (Fig. S3D,D'). Together, these data support the conclusion that *furina* is a strong candidate gene for the *loft* locus.

Although the above data suggested that *furina* is a candidate gene for the *loft* locus, we failed to identify any mutations in coding exons of the *furina* gene in mutants. To definitively determine whether deletion of *furina* caused *loft* mutant phenotypes, we generated a new *furina* mutant, *pku338*, using TALEN-based genome editing. A mutation of the *furina* gene was located in the propeptide region in *pku338* mutants, where five nucleotides were deleted and resulted in a short non-functional peptide (Fig. 3A). Similar to *loft* mutants, *pku338* mutants had an open-mouthed jaw (Fig. 3B,B'), lack of heart looping (Fig. 3C,C'), decreased DAF-2 DA-stained smooth muscle cells of the outflow tract (Fig. 3D,D') and a lack of paa budding (Fig. 3E,E'). We then investigated whether trans-heterozygous crosses between *loft* and *pku338* heterozygous zebrafish generated *loft* mutant phenotypes. As expected, ~25% of the offspring had *loft* phenotypes consisting of an open-mouthed jaw, abnormal heart looping, lack of differentiated smooth muscle cells in the outflow tract and paa budding (Fig. 3F-I'). Therefore, these genetic data confirmed that *furina* is fully responsible for the *loft* locus.

To determine the expression pattern of *furina* at cellular resolution during heart morphogenesis, we generated a *TgBAC(furina:GFP)* transgenic line in which a 29-kb *furina* promoter, derived from a *furina*-containing bacterial artificial chromosome (BAC) clone, was used to drive GFP reporter expression (Fig. S4A). This *furina* reporter

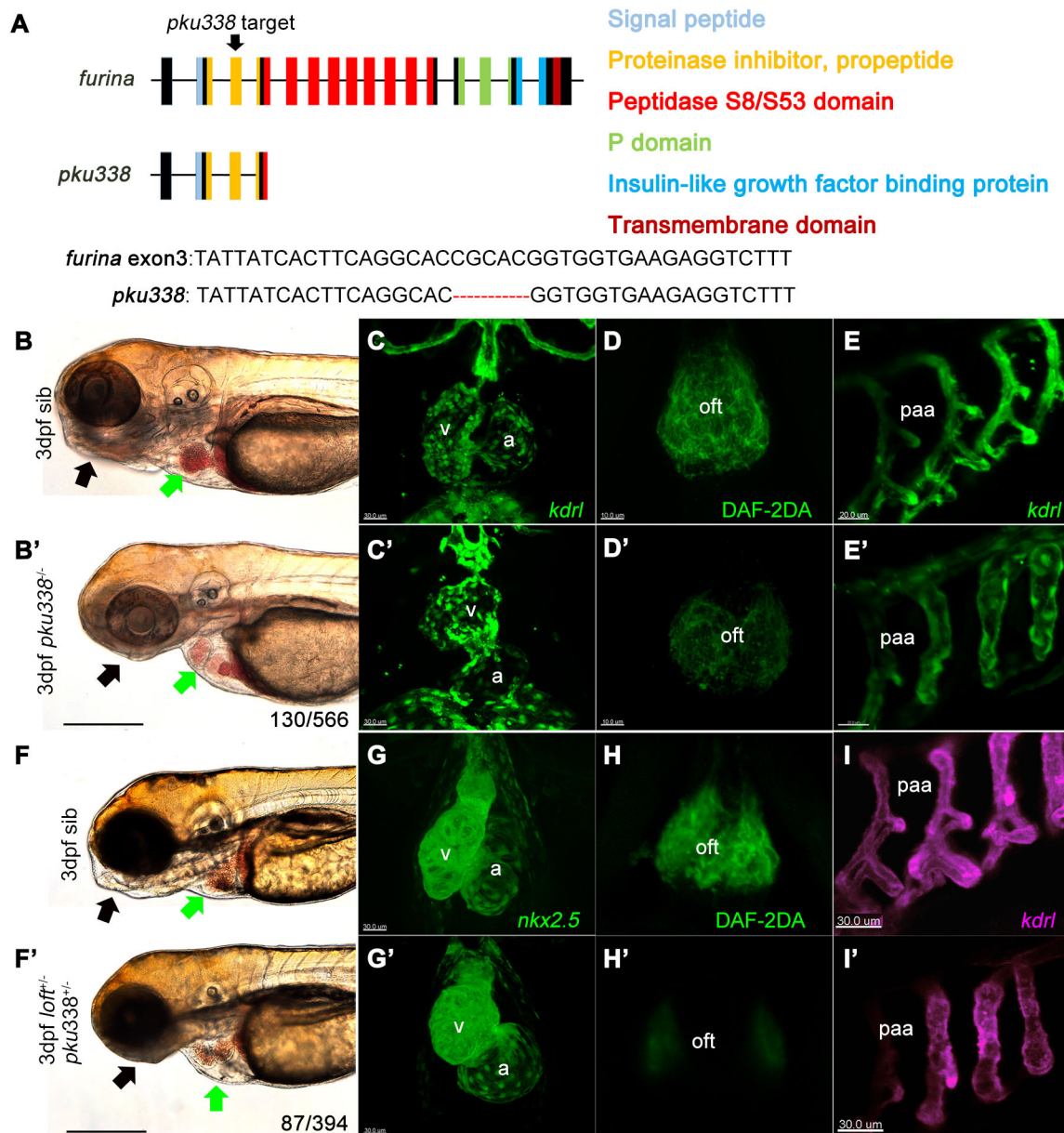


Fig. 3. Disruption of *furina* phenocopies *loft* mutant phenotypes. (A) Schematic showing wild-type Furina protein domains and truncated Furina protein from TALEN-induced *furina* mutant *pku338* (upper panels), as well as deletion of nucleotides 637 to 641 in *pku338* mutants, leading to out-of-frame translation after nucleotide 641 (lower panels). (B-E') Disruption of *furina* in *pku338* mutants resulted in the phenocopying of *loft* mutants, including open-mouth jaw (B'), abnormal heart looping (130/566) (C'), decreased NO in the outflow tract (D') and lack of paa budding (E') compared with siblings (B-E) at 3 dpf. (F-I') Heterozygous *loft* and heterozygous *pku338* mutants failed to complement, suggesting that *furina* is responsible for *loft* mutant phenotypes, of which interbreeding produced ~22% of embryos with an open-mouth jaw (F') and abnormal heart looping (87/394) (G'), as well as decreased NO in the outflow tract (H') and much reduced paa budding (I') compared with siblings (F-I) at 3 dpf. Black arrows indicate the jaw, and green arrows indicate the heart (B, B', F, and F'). a, atrium; oft, outflow tract; v, ventricle; Scale bars: 300 μ m (B, B', F, F'); 30 μ m (C, C', G, G', I, I'); 10 μ m (D, D', H, H'); 20 μ m (E, E').

revealed a broad expression pattern during zebrafish embryonic development, similar to that revealed by RNA *in situ* hybridization, and *furina* mRNA was enriched in *TgBAC(furina:GFP)* transgenic embryos (Fig. S4B-D). To determine the *furina*-expressing cell types in the embryonic heart, we crossed this *furina* reporter line with the cell-specific reporter lines epicardial-specific *Tg(tcf21:DsRed)*, myocardial-specific *Tg(my17:nucDsRed)* and vascular endothelial (endocardial)-specific *Tg(kdr1:mCherry)*. Confocal imaging revealed that *furina* colocalized with the epicardium (Fig. 4A-A"), myocardium (Fig. 4B-B") and endocardium (Fig. 4C-C") at 3 dpf.

Expression of *furina* in several cell types is consistent with its critical function during embryonic heart development.

Furina regulates heart looping and trabeculation via Notch signalling in zebrafish

Notch signalling is well known to play a critical role in vertebrate heart morphogenesis, and mutations of either Notch ligands or receptors leads to many congenital heart diseases (de la Pompa, 2009). Morpholino knockdown of *notch1b* in zebrafish leads to defects in both myocardial trabeculation and heart looping (Samsa

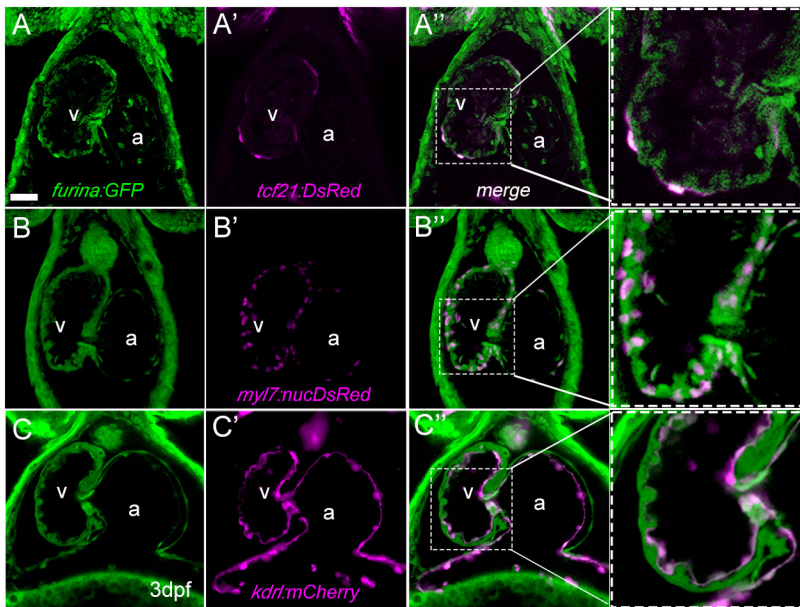


Fig. 4. *furina* is expressed in the epicardium, myocardium and endocardium. *TgBAC(furina:GFP)* expression (A-C) was colocalized with the epicardium marker *Tg(tcf21:DsRed)* (A-A'), the myocardium marker *Tg(myl7:nucDsRed)* (B-B') and the endocardium marker *Tg(kdrl:mCherry)*, with notably strong expression in the AVC (C-C'). The panels on the right of A'-C' are high magnification images of the indicated regions (boxes) in A'-C'. a, atrium; v, ventricle. Scale bar: 50 μ m (A-A'); 30 μ m (B-C').

et al., 2015). Thus, we used the *Tg(tp1:mCherry)* Notch reporter to address whether Notch signalling is compromised in *loft* mutants. We found much weaker *Tg(tp1:mCherry)* Notch signals in *loft* mutants than in siblings at 3 dpf (Fig. 5A,B). Using whole-mount *in situ* hybridization, we then assessed the expression patterns of four Notch receptor genes and found that only *notch1b*, but not *notch1a*, *notch2* or *notch3*, was detected in embryonic hearts at 3 dpf (Fig. 5C-F). Transcriptome analysis of ventricles from *loft* mutants and siblings also revealed similar results (Table S1). On the other hand, the level of *notch1b* mRNA was comparable in *loft* mutants and siblings (Fig. 5G,H). These data suggest that decreased Notch signalling in *loft* mutants is due to post-transcriptional or translational modifications of Notch1b.

The proprotein convertase Furin functions by enzymatic cleavage to remove the proprotein domains of its substrates. Previous work has demonstrated that rat Notch1 is one of the substrates of Furin (Bush et al., 2001). To address whether Furina also catalyzes the cleavage processing of Notch1b proteins in the zebrafish heart, we first determined the colocalization of *TgBAC(furina:GFP)* and *Tg(tp1:mCherry)* Notch reporter expression. The colocalization was particularly enriched in the AVC (Fig. 5I), suggesting that Furina and Notch1b are both expressed in endocardial cells, and thus Furina may act via the enzymatic cleavage of Notch1b receptors.

Homologous alignment of Notch1 proteins from several organisms revealed that zebrafish Notch1b has a conserved Furin recognition and cleavage site (R-X-X-R; Fig. S5A). As zebrafish Notch1b has a long epidermal growth factor (EGF)-like repeat domain, leading to a large molecular-weight protein, it is quite challenging to assess the full-length protein *in vivo* or *in vitro*. We thus generated a short-form Notch1b construct (Notch1b Δ N), in which the EGF-like repeats and PEST domains were replaced with EGFP and a Myc tag (Fig. S5C); a Furina-Notch1b construct (Furina-Notch1b Δ N) fusing Furina to Notch1b Δ N (Fig. S5D), as well as a mutated Notch1b construct (Furina-mtNotch1b Δ N), in which the Furina recognition site in the Furina-Notch1b Δ N construct was mutated from 'RKRR' to 'AAAA' (Fig. S5E). These constructs were transfected into HEK293T cells and subjected to western blot analysis, and a cleaved Notch1b peptide was evident in Furina-Notch1b Δ N-transfected cells, but not in Furina-mtNotch1b Δ N, control or Notch1b Δ N-transfected cells

(Fig. 6A), demonstrating that Furina is sufficient to cleave Notch1b and this cleavage is dependent on the enzymatic activity of Furina in zebrafish.

To address whether Notch signalling functions downstream from Furina, we applied conditional overexpression of N1bICD-EGFP (Notch1b intracellular domain fused with EGFP) driven by the zebrafish heat shock promoter in *loft* mutants. To visualize the trabeculae clearly, the *Tg(myl7:nucDsRed)* and *Tg(myl7:Ras-GFP)* transgenic lines were used to label nuclei and cell membranes of cardiomyocytes, respectively. Consistently, we found that transient overexpression of N1bICD by heat shock at 24 hpf, in which GFP signal could be detected 2 h later and lasted until 48 hpf, partially rescued both the heart looping and trabeculation defects in mutants compared with heat shock controls (Fig. 6B-E). Thus, our data suggest that cleavage processing of Notch1b by Furina might be required for both heart looping and trabeculation in zebrafish embryos.

To determine whether abnormal cardiac jogging affects heart looping development in *loft* mutants, we examined cardiac looping development after MK-0752 treatment at 24 hpf, when the early left-right asymmetry/cardiac jogging took place. MK-0752 is a potent and specific γ -secretase inhibitor (Krop et al., 2012), and its efficacy was confirmed by using *Tg(tp1:VenusPEST)* Notch reporter transgenic embryos (Fig. S6A,B). γ -secretase has the crucial proteolytic activity that releases the NICD to activate the Notch signalling pathway. We treated wild-type embryos at 24 hpf with 5 μ M MK-0752 and found that the treated embryos had more cardiac looping defects than the control DMSO group, suggesting that heart looping development is likely independent of cardiac jogging (Fig. S6C-E). To explore whether *furina* and *notch1b* synergistically regulate heart looping development, we found that a low concentration of MK-0752 (1 μ M) caused few heart looping defects for wild-type embryo, and DMSO treatment also caused few heart looping defects for embryos from wild-type and heterozygous *loft* crossings. However, 1 μ M MK-0752 treatment caused much more heart looping defects for embryos from wild-type and heterozygous *loft* crossings (Fig. S6F). Together, these data suggest that Furina synergistically acts with Notch signalling to regulate heart looping development that is independent of cardiac jogging during heart development.

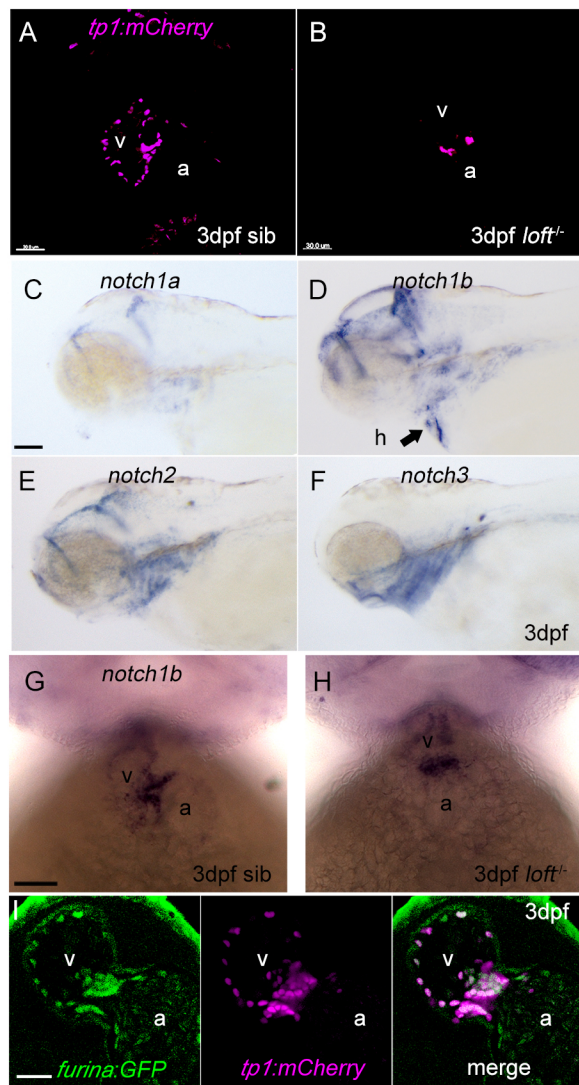


Fig. 5. Notch signalling is affected in *loft* mutants. (A,B) Notch reporter *Tg(tp1:mCherry)* decreased in *loft* mutant hearts (B) compared with siblings (A) at 3 dpf. (C-F) RNA *in situ* hybridization with probes of *notch* receptor genes revealed that only *notch1b*, but not *notch1a*, *notch2* and *notch3*, was expressed in the zebrafish heart at 3 dpf. (G,H) RNA *in situ* hybridization showed that *notch1b* mRNA was comparably expressed in *loft* mutants (H) and siblings (G) at 3 dpf. (I) The *Tg(tp1:mCherry)* Notch reporter was highly colocalized with *TgBAC(furina:GFP)* expression domains, particularly in the AVC. a, atrium; h, heart; v, ventricle. Scale bars: 30 μ m (A,B,I); 100 μ m (C-H).

DISCUSSION

In this study, unbiased ENU-induced mutagenesis of the zebrafish genome resulted in the isolation of the *loft* mutant, which showed evident defects in the cardiac outflow tract, heart looping and trabeculation, and craniofacial and paa defects at 3 dpf. Genetic, transgenic and epistatic analyses revealed that *furina* is the defective gene in *loft* mutants and is expressed in the epicardium, endocardium and myocardium. Mechanistic studies demonstrated that Furina catalyzes the cleavage processing of Notch1b proteins in cultured cells, suggesting a potential role of the Furina-Notch1b axis in regulating cardiac looping and trabecular development. Therefore, beyond previous reports on *furin* mutants in mice and zebrafish, we present evidence for a new layer of post-translational modification of Notch1b protein via Furina and thus highlight the function of the Furina-Notch1b axis in cardiac looping and trabeculation.

Furin, a proprotein convertase, is broadly expressed in the extra-embryonic and embryonic regions in mice. *Furin*-deficient mice die between E10.5 and E11.5 due to defects in early embryonic patterning, heart tube fusion and cardiac looping morphogenesis (Constam and Robertson, 2000; Roebroek et al., 1998). Endothelial-specific *Furin* knockout in mice leads to ventricular septal defects and valve malformations (Kim et al., 2012). These early studies in mice suggested that *Furin* was critical for heart morphogenesis, but its cellular and molecular mechanisms were not fully addressed. The zebrafish *furin* gene is duplicated to form two genes, *furina* and *furinb*. A zebrafish *furina* mutant, *sturgeon*, has been cloned to show that Furina regulates craniofacial patterning via modulating endothelin-1 signalling, which explains its open-mouthed jaw phenotype (Walker et al., 2006). The zebrafish mutant *ace of hearts* has left-right asymmetry defects and encodes *furina* (Tessadori et al., 2015). Furina regulates Nodal signalling by catalyzing the cleavage processing of Spaw proproteins during early embryogenesis. Although the left-right asymmetry defects in zebrafish often lead to a heart looping deficiency, it remains unclear whether the morphogenesis of heart looping is dependent on the early left-right asymmetry. Indeed, previous works have reported that abnormal left-right asymmetry and heart jogging do not always lead to looping defects (Bakkers et al., 2009; Chin et al., 2000; Ocana et al., 2017), supporting the notion that cardiac jogging and looping might be independently regulated. Thus, we hypothesized that Furina might regulate heart looping and/or trabeculation by modulating and activating other targeted proteins in the heart. We have shown that *notch1b*, but not other Notch receptor genes, is expressed in the embryonic heart; Furina is able to cleave Notch1b in cultured cells, and more importantly, conditional overexpression of zebrafish NICD (from Notch1b) partially rescues the looping (and trabeculation) defects in *loft* mutants. These data are consistent with previous reports that processing of Notch1 by Furin is required for activating Notch signalling components, including CSL [CBF1, Su(H) and LAG-1] and downstream targets (Bush et al., 2001). In addition, after cardiac jogging took place at 24 hpf, inhibition of the Notch signalling by γ -secretase inhibitor MK-0752 still caused cardiac looping defects. Thus, we provide evidence that Furina regulates cardiac looping and trabeculation probably by cleavage processing of Notch1b in zebrafish, which is likely independent of the left-right asymmetry/cardiac jogging, and this Furina-Notch1b axis signalling may extend to their function in mammalian heart morphogenesis.

The molecular mechanisms underlying cardiac looping remain incompletely understood. Some investigators have proposed that rotation of the heart tube driven by different rates of cardiomyocyte migration leads to looping (Baker et al., 2008; Bakkers et al., 2009). Others have considered that left-right differences in the proliferation rates of the second heart field control the direction of looping (Galli et al., 2008). It has been shown that mechanosensing and the myocardial cytoskeleton contribute to the bending and rotational forces during looping (Linask and Vanauker, 2007). Biophysical elements, cervical flexure and the splanchnopleure also generate rotational forces for looping (Ramasubramanian et al., 2013). Abnormal looping was highly penetrant in *loft* mutants, which was partially rescued by overexpression of NICD, and Furina and Notch1b synergistically regulate heart looping development independent of cardiac jogging, reaffirming the essential function of Furin-Notch signalling in heart looping. However, it is largely unknown how Notch signalling regulates looping. Primary cilia, which are hemodynamic force sensors, are required for endocardial Notch activation, and expanding cardiac jelly space occurs in

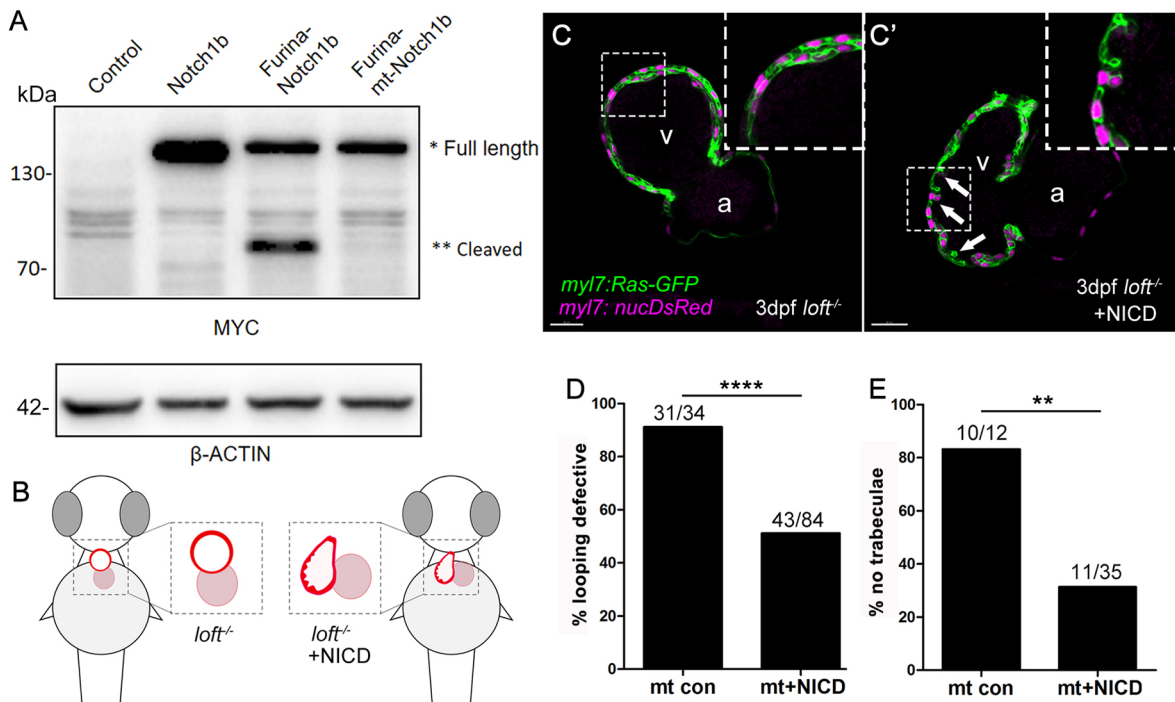


Fig. 6. Overexpression of NICD partially rescues *loft* mutant phenotypes. (A) Western blot revealed that Myc-tagged Notch1b Δ N was cleaved, but mutant Notch1b Δ N, in which the Furina cleavage sites were mutated, was not cleaved by Furina when both Furina and Notch1b Δ N or mutant Notch1b Δ N were co-expressed in 293T cells. (B) Cartoon images showing the defects of heart looping and trabeculation in *loft*^{-/-} mutants (left), which were rescued by the heat shock overexpression of NICD. (C,C') The defects of heart looping and trabeculation in *loft*^{-/-} mutants were partially rescued by overexpression of NICD (C') compared with mutant controls (C). The right upper corners are high magnification images of the boxed areas. (D,E) Overexpression of NICD in *loft* mutants partially rescued heart looping defects (43/84) (D) and trabeculation defects (11/35) (E), whereas most of the heat shock control mutant embryos exhibited heart looping defects (31/34) (D) and trabeculation defects (10/12) (E). *Tg(myl7:nucDsRed)* and *Tg(myl7:Ras-GFP)* were used to label nuclei and cell membranes of cardiomyocytes, respectively. White arrows point to trabecular cardiomyocytes. ***P*<0.01, *****P*<0.0001 (χ^2 test). a, atrium; v, ventricle. Scale bars: 30 μ m (C,C').

notch1b morphants in zebrafish (Samsa et al., 2015) and NFAT1: Cre; Notch1^{fl/fl} mouse mutants (Del Monte-Nieto et al., 2018), implying that Notch signalling regulates looping by transmitting shear stress forces from endocardium to myocardium. Future studies are needed to clarify the molecular role of Notch signalling in heart looping morphogenesis.

In addition to cardiac looping and trabeculation defects, the *loft* mutant exhibits evident defects in the jaws, pharyngeal arch artery budding and outflow tract smooth muscle differentiation, suggesting other roles of *furina* in regulating the development of the second heart field and cardiac neural crest cells. As we did not find apparent defects in the second heart field of *loft* mutants by examining the expression of transgenic reporters and marker genes, we turned our focus to the cardiac neural crest cells and found that their migration to the outflow tract was compromised and delayed. Notch signalling plays essential roles in the proliferation, migration and differentiation of cardiac neural crest cells. Although we found much reduced activity of Notch signalling in the pharyngeal arch artery region in *loft* mutants compared with siblings, overexpression of NICD was not able to rescue the defects in the jaw, pharyngeal arch artery budding or the outflow tract. We noted that *furina* was mainly expressed in the endothelium and epithelium of the pharyngeal arches, where Notch signalling was detected in the region surrounding the pharyngeal arch artery endothelia. These data suggest that Furina catalyzes the cleavage processing of substrates other than Notch1b to regulate cardiac neural crest cell development. This warrants further investigation.

Notch signalling is believed to be the central player in cardiac trabeculation by coordinating the expression of *efnb2b*, *neuregulin1*

and *bmp10* (Del Monte-Nieto et al., 2018; Grego-Bessa et al., 2007; Samsa et al., 2015). Cardiac contraction, primary cilia and shear stress via blood flow contribute to trabecular development by activating Notch signalling (Lee et al., 2016; Peshkovsky et al., 2011; Samsa et al., 2015). The peptidyl-prolyl isomerase Fkbp1a regulates cardiac trabeculation by decreasing NICD instability in mice (Chen et al., 2013). Although abnormal heart development has been reported in *furin* mutants in zebrafish and mice, neither the cellular nor the molecular abnormalities in the heart of *loft* mutants were clear. Our work has established the essential role of Furina-Notch1b signalling in cardiac trabeculation in zebrafish. In particular, we found that only overexpression of NICD induced early at 24 hpf, but not at 48 or 72 hpf (data not shown), partially rescued the trabeculation defects in *loft* mutants, which is consistent with the finding that early endocardial Notch activity is essential for cardiac trabeculation (Jimenez-Amilburu et al., 2016; Staudt et al., 2014). Using the short-lived Notch reporter *Tg(tp1:VenusPest)* to characterize Notch gene expression during heart morphogenesis in zebrafish, investigators have reported that Notch activity is mainly enriched in the endocardium from 28 to 55 hpf, and is then restricted to the endocardium of the AVC until 4 weeks post-fertilization (Samsa et al., 2015). Notch activity is first detectable in the endocardium of mouse embryos around E7.5 (Del Monte et al., 2007). Endocardium-specific knockout of either Notch1 or RBPJk in mice results in impaired cardiac trabeculation and fewer proliferating ventricular cardiomyocytes (D'Amato et al., 2016; Grego-Bessa et al., 2007; Luxan et al., 2016). In addition, some investigators have shown that myocardial Notch activity normally prevents cardiomyocyte sprouting and trabeculation by inhibiting

ErbB2 signalling from 72 to 96 hpf in zebrafish (Han et al., 2016), whereas others have argued that myocardial Notch activity is mainly essential for the maintenance of compact myocardium (Jimenez-Amilburu et al., 2016). Nevertheless, myocardium-specific knockout of the Notch signalling component *Mib1* in mice leads to a thin ventricular wall and an extensive trabecular network (Captur et al., 2016). Together with the early role of Notch signalling in the *loft* mutant, it is reasonable to conclude that sequential activation of Furina-Notch signalling, presumably initially in the endocardium and later in the myocardium, takes place during trabecular morphogenesis.

MATERIALS AND METHODS

Zebrafish stocks and husbandry

Zebrafish were raised at 28.5°C according to the animal protocol 'IMM-XiongJW-3' approved by the Peking University Animal Care and Use Committee, and in line with the Guide for the Care and Use of Laboratory Animals published by the National Institute of Health. The embryos were anaesthetized in Tricaine (A5040, Sigma-Aldrich) with a final concentration of 0.17 g/l. The *Tg(nkx2.5:zsYellow)* transgenic zebrafish were a gift from Dr Geoffrey Burns (Massachusetts General Hospital, Boston, MA, USA; Zhou et al., 2011); the *furina* mutant (*pku338*) was generated by TALEN-based genome editing as described below; *TgBAC(furina:GFP)(pku364)* was generated using the DNA recombination method (Yu et al., 2000); and *Tg(hsp70:N1bICD-GFP)(pku340)* was generated using Tol2-based transgenesis (Kawakami et al., 2004). Other zebrafish lines used in this study were: *loft* (*pku336*); AB; WIK; *Tg(kdrl:GFP)* (Beis et al., 2005); *Tg(tp1:mCherry)* (Parsons et al., 2009); *Tg(tp1:Venus-PEST)* (Ninov et al., 2012); *Tg(kdrl:mCherry)* (Jin et al., 2005); *Tg(tcf21:DsRed)* (Wang et al., 2011); *Tg(myf7:nucDsRed)* (Burns et al., 2005); and *Tg(myf7:Ras-GFP)* (Zhang et al., 2013).

Positional cloning of the *loft* locus

The *loft* mutant was isolated from a stock of zebrafish that was subjected to unbiased ENU-induced mutagenesis of the AB zebrafish genome, which was originally designed to isolate bloodless mutants, at the laboratory of Dr Barry Paw at Brigham Women's Hospital and Harvard Medical School (Shah et al., 2012). Positional cloning was performed as described previously (Lei et al., 2017). Briefly, the *loft* locus was mapped to chromosome 7 using genetic linkage analysis with single-strand length polymorphism genetic markers, and further genetic walking and physical mapping were based on public databases of the zebrafish genome (ZV8 and ZV9) (Kettleborough et al., 2013). The primer sequences of genetic markers are listed in Table S2. The genetic interval of *loft* was determined between markers AF-10 and zgc112142-13 (Fig. 2A), in which two genes, *slc39a1* and *furina*, were identified. The coding region of the two cDNAs were then subjected to Sanger sequencing. To further confirm candidate genes, we performed whole-mount *in situ* hybridization, microinjection of mRNA for rescuing mutant phenotypes and microinjection of morpholino for phenocopying mutant phenotypes as described previously (Lei et al., 2017).

Generation of the TALEN-induced *furina* mutant *pku338*

Furina TALEN targets (Table S5), primarily consisting of 12-17-bp recognition sites, 3'T and 12-21-bp spacer sites with a unique restriction enzyme site, were designed using an online tool (<http://boglabx.plp.iastate.edu/TALENT/>). The construction of TALEN pairs was carried out as described previously (Yang et al., 2013). TALEN mRNA pairs were mixed (100 ng/μl each) and injected into one-cell-stage zebrafish embryos. We screened half of the injected embryos for *furina* mutations using enzyme digestion analysis of their genomic DNA. The other half of the injected embryos was raised to adulthood, and heritable mutations were further confirmed by genotyping F₁ embryos. Mutations were confirmed by Sanger sequencing.

Morpholino and mRNA injection

The *furina* cDNA was amplified from cDNA libraries of wild-type AB zebrafish embryos and cloned into pXT7 vector (Table S4). Capped mRNA of *furina* was synthesized using an mMESSAGE mMACHINE T7 high yield capped RNA transcription kit (AM1344, Ambion). Approximately 2 nl of 100 ng/μl *furina* mRNA was injected into one-cell-stage embryos from crosses of heterozygous *loft* zebrafish with or without a *Tg(kdrl:GFP)* transgenic background. Injected embryos were scored for cardiovascular phenotypes at 3 dpf. An ATG morpholino of *furina* (5'-CCACCTGCTGTTCGCCACATTAC-3') was designed and purchased from Gene Tools (Philomath, OR, USA).

In situ RNA hybridization

Whole-mount *in situ* RNA hybridization was performed as described previously (Lei et al., 2017). Briefly, the T7 promoter was introduced into PCR fragments of *furina*, *notch1a*, *notch1b*, *notch2* and *notch3* that were amplified from cDNA libraries of wild-type AB embryos, and digoxigenin-labelled probes were synthesized using T7 RNA polymerase (10881767001, Roche). The primer sequences for generating *in situ* hybridization probes are listed in Table S3.

DAF-2 DA staining

Nitric oxide in the outflow tract was determined using DAF-2 DA staining as described previously (Grimes et al., 2006). Zebrafish embryos at 48 hpf were incubated in E3 with 10 μM DAF-2 DA (D225, Sigma-Aldrich) for 12 h.

Quantitative real-time PCR

Total RNA from *loft* mutants and their siblings at 48 hpf was isolated using TRI reagent (93289, Sigma-Aldrich), and the first strand of cDNA was synthesized for quantitative real-time PCR (18080051, Invitrogen). GAPDH was used to normalize *furina* expression levels (Table S4). The statistical significance between two groups was calculated using an unpaired Student's *t*-test, with a two-tailed *P*-value.

RNA-seq

The cDNA libraries of *loft* mutants or siblings were constructed according to the manufacturer's instructions (KT110700424, Yikon Genomics). Briefly, at 3 dpf, when the *loft* mutants and siblings can be separated easily, the ventricles of *loft* mutants or siblings were isolated and added into cell lysis buffer in a PCR tube. The sample was then incubated at 70°C in a thermal cycler. Reverse transcriptase enzyme mix was then added into the lysed sample and a reverse transcription reaction was performed. Next, MALBAC pre-amplification and exponential amplification was carried out in a thermal cycler. The amplified cDNA libraries were purified by Ampure XP magnetic beads (A63880, Agencourt). After confirming the quality and integrity of the cDNA libraries using a Fragment Analyzer system, RNA-seq was carried out using Illumina HiSeq 2500 to generate 100-bp pair-end reads for each sample. Low-quality reads and sequencing adapters were removed from the raw sequencing data, and the clean reads were mapped onto the zebrafish transcriptome.

Construction of the *furina* BAC reporter *TgBAC(furina:GFP)*

The *TgBAC(furina:GFP)* line was generated based on two protocols (Lee et al., 2001; Suster et al., 2011). Briefly, the *furina* promoter-containing BACCH211-194N16 was transfected into DY380, which has a modified chromosome consisting of elements for DNA recombination (Yu et al., 2000). The GFP-KAN fragment was amplified with 50-bp homologous sequences and then recombined into the BAC by replacing a region of 500 bp downstream from the *furina* ATG start codon. A BAC fragment of ~30 kb containing 29 kb *furina* promoter and 1 kb GFP-KAN reporter was subcloned into the PNPC2 plasmid to form the *furina:GFP* construct, which contained I-Sce I sites (Fig. S3; Table S4). The *furina:GFP* construct was injected into one-cell-stage embryos with meganuclease (Fermentas, Waltham, MA, USA), and injected embryos with GFP signals were then raised to F₀ adults. F₀ zebrafish were crossed with wild-type TL to obtain F₁ embryos for identifying *furina:GFP* germline transmission. We isolated

three transgenic lines that showed identical GFP expression patterns during early embryogenesis. They were named transgenic lines *pku364*, *pku365* and *pku366*, and *pku364* was primarily used in this work.

To isolate GFP⁺ cells, *TgBAC(furina:GFP)* transgenic embryos were obtained by crossing GFP heterozygous male zebrafish with TU females. The offspring that exhibited green fluorescence were collected at 1 dpf. Embryos at 2 dpf were dissociated into single cells using Accutase (A6864, Sigma-Aldrich) at 28.5°C. The GFP⁺ and GFP⁻ cells were sorted using a BD FACSAria SORP Flow Cytometer Cell Sorter. Quantitative real-time PCR was performed with the sorted cells.

Construction of expression plasmid clones of Notch1b and its mutant variants

notch1b and *furina* cDNA were amplified from cDNA libraries of zebrafish embryos at 3 dpf. To facilitate biochemical analysis of Notch1b and its variants based on a previous report in mice (Mumm et al., 2000), the N-terminal EGF-like repeats and the 289 most C-terminal residues (Leu-2194 to the C terminus) of Notch1b were replaced with EGFP and a Myc tag, respectively. *furina* cDNA with a T2A sequence was cloned into the Notch1bΔN construct to fuse with the 5' GFP sequence (E2621, New England Biolabs). Site-directed mutagenesis (FM111, TransGen) in Notch1bΔN was carried out to change the Furin recognition amino acids RQRR to AAAA to form the Furina-*mt* Notch1bΔN construct as described previously (Logeat et al., 1998). These cDNA clones were cloned into the pEGFP-C1 vector (Table S4).

Cell culture, transfection and western blotting

HEK293T cells (American Type Culture Collection) were grown in Dulbecco's modified Eagle's high glucose medium (SH30019, HyClone). Cells were tested negative for mycoplasma contamination. Plasmids were transfected with Lipofectamine 3000 (L3000001, Invitrogen), and transfected cells were grown for 60 h and then lysed by RIPA lysis buffer (C1055, Applygen) for subsequent western blotting. The following antibodies were used: mouse monoclonal antibody to Myc-Tag (AT0023, CMCTAG); recombinant rabbit monoclonal antibody to actin (ET1701-80, HuaBio); goat anti-rabbit IgG(H+L)-horseradish peroxidase (HRP) (BE0101, Easybio); and goat anti-mouse IgG (H&L)-HRP (BE0102, Easybio). Primary antibodies were used at a dilution of 1:1000. Secondary antibodies were used at a dilution of 1:10,000.

Generating the *Tg(hsp70l:N1bICD-EGFP)* transgenic line and N1bICD rescue assay

The *Tg(hsp70l:N1bICD-EGFP)^{pku340}* line was generated using Tol2-based transgenesis (Kawakami et al., 2004), in which the zebrafish N1bICD-EGFP fusion gene is driven by the heat shock cognate 70-kd protein-like (*hsp70l*) promoter. Compound zebrafish containing heterozygous *loft* and *Tg(hsp70l:N1bICD-EGFP)^{pku340}* were generated (Table S4). To test whether overexpression of N1bICD-EGFP was able to rescue *loft* mutant phenotypes, we crossed *loft^{+/-}* zebrafish with *loft^{+/-}; Tg(hsp70l:N1bICD-EGFP)^{tg/tg}* zebrafish to obtain ~25% embryos with *loft^{-/-}; Tg(hsp70l:N1bICD-EGFP)^{tg/tg}*, and ~75% (wild type and *loft^{+/-}*) embryos with *Tg(hsp70l:N1bICD-EGFP)^{tg/tg}*. These embryos were to heat shock (37°C) for 20 min to induce N1bICD expression. We then scored abnormal cardiac looping and trabeculation of the above two groups of embryos at 3 dpf. Genotyping of embryos was determined by RT-PCR, as *furina* is almost not expressed in *loft* mutants (Fig. 2B).

Confocal imaging of zebrafish embryos

Zebrafish embryos were mounted in 1.5% low-melting agarose, and images were captured using an LSM700 confocal microscope (Zeiss, Oberkochen, Germany) according to the manufacturer's instructions, as described previously (Lei et al., 2017).

MK-0752 treatment

MK-0752 (HY-10974, MedChemExpress) is a potent and specific γ -secretase inhibitor. Its powder was dissolved in DMSO to make 20 mM stock solutions. Final concentrations used for zebrafish embryos were 5 μ M

and 1 μ M. Wild-type or *Tg(tp1:Venus-PEST)* heterozygous transgenic embryos at 24 hpf were treated with either DMSO or MK-0752 when cardiac jogging took place. Cardiac looping defects were scored under a microscope at 3 dpf.

Statistical analysis

Sample sizes, statistical tests and *P*-values are indicated in the figures or the legends. The statistical significance between two groups was determined using a paired Student's *t*-test, with a two-tailed *P*-value, and the data were reported as mean \pm s.d. χ^2 tests were used where appropriate. **P*<0.05; ***P*<0.01; ****P*<0.001; *****P*<0.0001.

Acknowledgements

We thank Drs Jiaojiao Zhang, Jing Xu and Barry Paw for initial isolation and mapping of the *loft* mutant; Drs Yanmei Liu and Chuanmao Zhang for providing plasmid clones; Drs Geoff Burns, Michael Parsons and Rulin Zhang for providing transgenic lines; and Dr Iain C. Bruce for critical comments and reading the manuscript.

Competing interests

The authors declare no competing or financial interests.

Author contributions

Methodology: H.Z., W.W., G.P.; Validation: S.-S.C., L.G., R.Y.; Investigation: Q.Z., L.L., S.-S.C., L.G., R.Y.; Writing - original draft: Q.Z., L.L.; Writing - review & editing: J.-W.X.; Supervision: X.Z., J.-W.X.; Funding acquisition: X.Z., J.-W.X.

Funding

This work was supported by grants from the National Key Research and Development Program of China (2019 YFA0801602 and 2018YFA0800501); the National Natural Science Foundation of China (31730061, 31430059 and 81870198); and AstraZeneca (Asia and Emerging Markets, Innovative Medicines and Early Development).

Data availability

RNA-seq data has been deposited to the sequence read archive (SRA) under BioProject accession number PRJNA773625.

References

- Baker, K., Holtzman, N. G. and Burdine, R. D. (2008). Direct and indirect roles for Nodal signaling in two axis conversions during asymmetric morphogenesis of the zebrafish heart. *Proc. Natl. Acad. Sci. USA* **105**, 13924-13929. doi:10.1073/pnas.0802159105
- Bakkers, J., Verhoeven, M. C. and Abdelilah-Seyfried, S. (2009). Shaping the zebrafish heart: from left-right axis specification to epithelial tissue morphogenesis. *Dev. Biol.* **330**, 213-220. doi:10.1016/j.ydbio.2009.04.011
- Beis, D., Bartman, T., Jin, S.-W., Scott, I. C., D'Amico, L. A., Ober, E. A., Verkade, H., Frantsve, J., Field, H. A., Wehman, A. et al. (2005). Genetic and cellular analyses of zebrafish atrioventricular cushion and valve development. *Development* **132**, 4193-4204. doi:10.1242/dev.01970
- Burns, C. G., Milan, D. J., Grande, E. J., Rottbauer, W., MacRae, C. A. and Fishman, M. C. (2005). High-throughput assay for small molecules that modulate zebrafish embryonic heart rate. *Nat. Chem. Biol.* **1**, 263-264. doi:10.1038/nchembio732
- Bush, G., diSibio, G., Miyamoto, A., Denault, J.-B., Leduc, R. and Weinmaster, G. (2001). Ligand-induced signaling in the absence of furin processing of Notch1. *Dev. Biol.* **229**, 494-502. doi:10.1006/dbio.2000.9992
- Captur, G., Wilson, R., Bennett, M. F., Luxán, G., Nasis, A., de la Pompa, J. L., Moon, J. C. and Mohun, T. J. (2016). Morphogenesis of myocardial trabeculae in the mouse embryo. *J. Anat.* **229**, 314-325. doi:10.1111/joa.12465
- Chen, H., Zhang, W., Sun, X., Yoshimoto, M., Chen, Z., Zhu, W., Liu, J., Shen, Y., Yong, W., Li, D. et al. (2013). Fkbp1a controls ventricular myocardium trabeculation and compaction by regulating endocardial Notch1 activity. *Development* **140**, 1946-1957. doi:10.1242/dev.089920
- Cherian, A. V., Fukuda, R., Augustine, S. M., Maischein, H.-M. and Stainier, D. Y. R. (2016). N-cadherin relocalization during cardiac trabeculation. *Proc. Natl. Acad. Sci. USA* **113**, 7569-7574. doi:10.1073/pnas.1606385113
- Chin, A. J., Tsang, M. and Weinberg, E. S. (2000). Heart and gut chiralities are controlled independently from initial heart position in the developing zebrafish. *Dev. Biol.* **227**, 403-421. doi:10.1006/dbio.2000.9924
- Constam, D. B. and Robertson, E. J. (2000). Tissue-specific requirements for the proprotein convertase furin/SPC1 during embryonic turning and heart looping. *Development* **127**, 245-254. doi:10.1242/dev.127.2.245
- D'Amato, G., Luxán, G., del Monte-Nieto, G., Martínez-Poveda, B., Torroja, C., Walter, W., Bochter, M. S., Benedetto, R., Cole, S., Martínez, F. et al. (2016). Sequential Notch activation regulates ventricular chamber development. *Nat. Cell Biol.* **18**, 7-20. doi:10.1038/ncb3280

- de la Pompa, J. L. (2009). Notch signaling in cardiac development and disease. *Pediatr. Cardiol.* **30**, 643-650. doi:10.1007/s00246-008-9368-z
- de la Pompa, J. L. and Epstein, J. A. (2012). Coordinating tissue interactions: Notch signaling in cardiac development and disease. *Dev. Cell* **22**, 244-254. doi:10.1016/j.devcel.2012.01.014
- Del Monte, G., Grego-Bessa, J., González-Rajal, A., Bolós, V. and De La Pompa, J. L. (2007). Monitoring Notch1 activity in development: evidence for a feedback regulatory loop. *Dev. Dyn.* **236**, 2594-2614. doi:10.1002/dvdy.21246
- Del Monte-Nieto, G., Ramalison, M., Adam, A. A. S., Wu, B., Aharonov, A., D'Uva, G., Bourke, L. M., Pitulescu, M. E., Chen, H., de la Pompa, J. L. et al. (2018). Control of cardiac jelly dynamics by NOTCH1 and NRG1 defines the building plan for trabeculation. *Nature* **557**, 439-445. doi:10.1038/s41586-018-0110-6
- Evans, S. M., Yelon, D., Conlon, F. L. and Kirby, M. L. (2010). Myocardial lineage development. *Circ. Res.* **107**, 1428-1444. doi:10.1161/CIRCRESAHA.110.227405
- Galli, D., Domínguez, J. N., Zaffran, S., Munk, A., Brown, N. A. and Buckingham, M. E. (2008). Atrial myocardium derives from the posterior region of the second heart field, which acquires left-right identity as *Pitx2c* is expressed. *Development* **135**, 1157-1167. doi:10.1242/dev.014563
- Grego-Bessa, J., Luna-Zurita, L., del Monte, G., Bolós, V., Melgar, P., Arandilla, A., Garratt, A. N., Zang, H., Mukoyama, Y.-S., Chen, H. et al. (2007). Notch signaling is essential for ventricular chamber development. *Dev. Cell* **12**, 415-429. doi:10.1016/j.devcel.2006.12.011
- Grimes, A. C., Stadt, H. A., Shepherd, I. T. and Kirby, M. L. (2006). Solving an enigma: arterial pole development in the zebrafish heart. *Dev. Biol.* **290**, 265-276. doi:10.1016/j.ydbio.2005.11.042
- Han, P., Bloomekatz, J., Ren, J., Zhang, R., Grinstein, J. D., Zhao, L., Burns, C. G., Burns, C. E., Anderson, R. M. and Chi, N. C. (2016). Coordinating cardiomyocyte interactions to direct ventricular chamber morphogenesis. *Nature* **534**, 700-704. doi:10.1038/nature18310
- Jiménez-Amilburu, V., Rasouli, S. J., Staudt, D. W., Nakajima, H., Chiba, A., Mochizuki, N. and Stainier, D. Y. R. (2016). In vivo visualization of cardiomyocyte apicobasal polarity reveals epithelial to mesenchymal-like transition during cardiac trabeculation. *Cell Rep.* **17**, 2687-2699. doi:10.1016/j.celrep.2016.11.023
- Jin, S.-W., Beis, D., Mitchell, T., Chen, J.-N. and Stainier, D. Y. R. (2005). Cellular and molecular analyses of vascular tube and lumen formation in zebrafish. *Development* **132**, 5199-5209. doi:10.1242/dev.02087
- Kawakami, K., Takeda, H., Kawakami, N., Kobayashi, M., Matsuda, N. and Mishina, M. (2004). A transposon-mediated gene trap approach identifies developmentally regulated genes in zebrafish. *Dev. Cell* **7**, 133-144. doi:10.1016/j.devcel.2004.06.005
- Kelly, R. G., Buckingham, M. E. and Moorman, A. F. (2014). Heart fields and cardiac morphogenesis. *Cold Spring Harb. Perspect. Med.* **4**, a015750. doi:10.1101/cshperspect.a015750
- Kettleborough, R. N. W., Busch-Nentwich, E. M., Harvey, S. A., Dooley, C. M., de Brijn, E., van Eeden, F., Sealy, I., White, R. J., Herd, C., Nijman, I. J. et al. (2013). A systematic genome-wide analysis of zebrafish protein-coding gene function. *Nature* **496**, 494-497. doi:10.1038/nature11992
- Kim, W., Essalmani, R., Szumska, D., Creemers, J. W. M., Roebroek, A. J. M., D'Orleans-Juste, P., Bhattacharya, S., Seidah, N. G. and Prat, A. (2012). Loss of endothelial furin leads to cardiac malformation and early postnatal death. *Mol. Cell. Biol.* **32**, 3382-3391. doi:10.1128/MCB.06331-11
- Krop, I., Demuth, T., Guthrie, T., Wen, P. Y., Mason, W. P., Chinnaiyan, P., Butowski, N., Groves, M. D., Kesari, S., Freedman, S. J. et al. (2012). Phase I pharmacologic and pharmacodynamic study of the gamma secretase (Notch) inhibitor MK-0752 in adult patients with advanced solid tumors. *J. Clin. Oncol.* **30**, 2307-2313. doi:10.1200/JCO.2011.39.1540
- Lee, E.-C., Yu, D., Martínez de Velasco, J., Tessarollo, L., Swing, D. A., Court, D. L., Jenkins, N. A. and Copeland, N. G. (2001). A highly efficient *Escherichia coli*-based chromosome engineering system adapted for recombinogenic targeting and subcloning of BAC DNA. *Genomics* **73**, 56-65. doi:10.1006/geno.2000.6451
- Lee, J., Fei, P., Packard, R. R. S., Kang, H., Xu, H., Baek, K. I., Jen, N., Chen, J., Yen, H., Kuo, C.-C. J. et al. (2016). 4-Dimensional light-sheet microscopy to elucidate shear stress modulation of cardiac trabeculation. *J. Clin. Invest.* **126**, 1679-1690. doi:10.1172/JCI83496
- Lei, L., Yan, S.-Y., Yang, R., Chen, J.-Y., Li, Y., Bu, Y., Chang, N., Zhou, Q., Zhu, X., Li, C.-Y. et al. (2017). Spliceosomal protein *etfud2* mutation leads to p53-dependent apoptosis in zebrafish neural progenitors. *Nucleic Acids Res.* **45**, 3422-3436. doi:10.1093/nar/gkw1043
- Lin, X. and Xu, X. (2009). Distinct functions of Wnt/ β -catenin signaling in KV development and cardiac asymmetry. *Development* **136**, 207-217. doi:10.1242/dev.029561
- Linask, K. K. and Vanauker, M. (2007). A role for the cytoskeleton in heart looping. *ScientificWorldJournal* **7**, 280-298. doi:10.1100/tsw.2007.87
- Loquat, F., Bessia, C., Brou, C., LeBail, O., Jarriault, S., Seidah, N. G. and Israel, A. (1998). The Notch1 receptor is cleaved constitutively by a furin-like convertase. *Proc. Natl. Acad. Sci. USA* **95**, 8108-8112. doi:10.1073/pnas.95.14.8108
- Luxán, G., D'Amato, G., MacGrogan, D. and de la Pompa, J. L. (2016). Endocardial Notch signaling in cardiac development and disease. *Circ. Res.* **118**, e1-e18. doi:10.1161/CIRCRESAHA.115.305350
- Mumm, J. S., Schroeter, E. H., Saxena, M. T., Griesemer, A., Tian, X., Pan, D. J., Ray, W. J. and Kopan, R. (2000). A ligand-induced extracellular cleavage regulates γ -secretase-like proteolytic activation of Notch1. *Mol. Cell* **5**, 197-206. doi:10.1016/S1097-2765(00)80416-5
- Ninov, N., Borius, M. and Stainier, D. Y. R. (2012). Different levels of Notch signaling regulate quiescence, renewal and differentiation in pancreatic endocrine progenitors. *Development* **139**, 1557-1567. doi:10.1242/dev.076000
- Ocaña, O. H., Coskun, H., Minguilón, C., Murawala, P., Tanaka, E. M., Galcerán, J., Muñoz-Chápuli, R. and Nieto, M. A. (2017). A right-handed signalling pathway drives heart looping in vertebrates. *Nature* **549**, 86-90. doi:10.1038/nature23454
- Parsons, M. J., Pisharath, H., Yusuff, S., Moore, J. C., Siekmann, A. F., Lawson, N. and Leach, S. D. (2009). Notch-responsive cells initiate the secondary transition in larval zebrafish pancreas. *Mech. Dev.* **126**, 898-912. doi:10.1016/j.mod.2009.07.002
- Pedrazzini, T. (2007). Control of cardiogenesis by the notch pathway. *Trends Cardiovasc. Med.* **17**, 83-90. doi:10.1016/j.tcm.2007.01.003
- Peshkovsky, C., Totong, R. and Yelon, D. (2011). Dependence of cardiac trabeculation on neuregulin signaling and blood flow in zebrafish. *Dev. Dyn.* **240**, 446-456. doi:10.1002/dvdy.22526
- Ramasubramanian, A., Chu-Lagraff, Q. B., Buma, T., Chico, K. T., Carnes, M. E., Burnett, K. R., Bradner, S. A. and Gordon, S. S. (2013). On the role of intrinsic and extrinsic forces in early cardiac S-looping. *Dev. Dyn.* **242**, 801-816. doi:10.1002/dvdy.23968
- Roebroek, A. J., Umans, L., Pauli, I. G., Robertson, E. J., van Leuven, F., Van de Ven, W. J. and Constam, D. B. (1998). Failure of ventral closure and axial rotation in embryos lacking the proprotein convertase Furin. *Development* **125**, 4863-4876. doi:10.1242/dev.125.24.4863
- Samsa, L. A., Givens, C., Tzima, E., Stainier, D. Y. R., Qian, L. and Liu, J. (2015). Cardiac contraction activates endocardial Notch signaling to modulate chamber maturation in zebrafish. *Development* **142**, 4080-4091. doi:10.1242/dev.125724
- Seidah, N. G. (2011). What lies ahead for the proprotein convertases? *Ann. N. Y. Acad. Sci.* **1220**, 149-161. doi:10.1111/j.1749-6632.2010.05883.x
- Shah, D. I., Takahashi-Makise, N., Cooney, J. D., Li, L., Schultz, I. J., Pierce, E. L., Narla, A., Seguin, A., Hattangadi, S. M., Medlock, A. E. et al. (2012). Mitochondrial *Atf1p1* regulates haem synthesis in developing erythroblasts. *Nature* **491**, 608-612. doi:10.1038/nature11536
- Staudt, D. and Stainier, D. (2012). Uncovering the molecular and cellular mechanisms of heart development using the zebrafish. *Annu. Rev. Genet.* **46**, 397-418. doi:10.1146/annurev-genet-110711-155646
- Staudt, D. W., Liu, J., Thorn, K. S., Stuurman, N., Liebling, M. and Stainier, D. Y. R. (2014). High-resolution imaging of cardiomyocyte behavior reveals two distinct steps in ventricular trabeculation. *Development* **141**, 585-593. doi:10.1242/dev.098632
- Suster, M. L., Abe, G., Schouw, A. and Kawakami, K. (2011). Transposon-mediated BAC transgenesis in zebrafish. *Nat. Protoc.* **6**, 1998-2021. doi:10.1038/nprot.2011.416
- Tessadori, F., Noël, E. S., Rens, E. G., Magliozzi, R., Evers-van Gogh, I. J. A., Guardavaccaro, D., Merks, R. M. H. and Bakkers, J. (2015). Nodal signaling range is regulated by proprotein convertase-mediated maturation. *Dev. Cell* **32**, 631-639. doi:10.1016/j.devcel.2014.12.014
- van Tetering, G. and Vooijs, M. (2011). Proteolytic cleavage of Notch: "HIT and RUN". *Curr. Mol. Med.* **11**, 255-269. doi:10.2174/156652411795677972
- Wagner, M. and Siddiqui, M. A. (2007). Signal transduction in early heart development (II): ventricular chamber specification, trabeculation, and heart valve formation. *Exp. Biol. Med. (Maywood)* **232**, 866-880.
- Walker, M. B., Miller, C. T., Coffin Talbot, J., Stock, D. W. and Kimmel, C. B. (2006). Zebrafish furin mutants reveal intricacies in regulating Endothelin1 signaling in craniofacial patterning. *Dev. Biol.* **295**, 194-205. doi:10.1016/j.ydbio.2006.03.028
- Wang, J., Panáková, D., Kikuchi, K., Holdway, J. E., Gemberling, M., Burris, J. S., Singh, S. P., Dickson, A. L., Lin, Y.-F., Sabeh, M. K. et al. (2011). The regenerative capacity of zebrafish reverses cardiac failure caused by genetic cardiomyocyte depletion. *Development* **138**, 3421-3430. doi:10.1242/dev.068601
- Wu, M. (2018). Mechanisms of trabecular formation and specification during cardiogenesis. *Pediatr. Cardiol.* **39**, 1082-1089. doi:10.1007/s00246-018-1868-x
- Yang, J., Yuan, P., Wen, D., Sheng, Y., Zhu, S., Yu, Y., Gao, X. and Wei, W. (2013). ULTIMATE system for rapid assembly of customized TAL effectors. *PLoS ONE* **8**, e75649. doi:10.1371/journal.pone.0075649
- Yu, D., Ellis, H. M., Lee, E.-C., Jenkins, N. A., Copeland, N. G. and Court, D. L. (2000). An efficient recombination system for chromosome engineering in *Escherichia coli*. *Proc. Natl. Acad. Sci. USA* **97**, 5978-5983. doi:10.1073/pnas.100127597

Zhang, R., Han, P., Yang, H., Ouyang, K., Lee, D., Lin, Y.-F., Ocorr, K., Kang, G., Chen, J., Stainier, D. Y. R. et al. (2013). In vivo cardiac reprogramming contributes to zebrafish heart regeneration. *Nature* **498**, 497-501. doi:10.1038/nature12322

Zhou, Y., Cashman, T. J., Nevis, K. R., Obregon, P., Carney, S. A., Liu, Y., Gu, A., Mosimann, C., Sondalle, S., Peterson, R. E. et al. (2011). Latent TGF- β binding protein 3 identifies a second heart field in zebrafish. *Nature* **474**, 645-648. doi:10.1038/nature10094

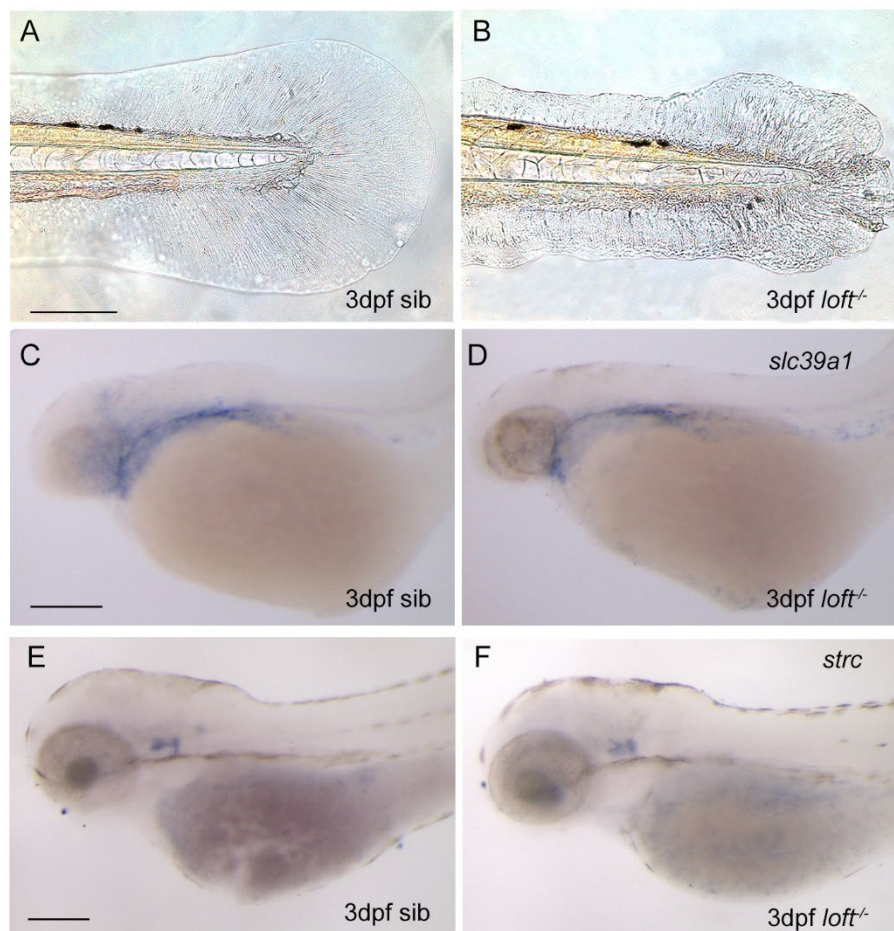


Fig. S1. The tail fin phenotype and the expression of *slc39a1* and *strc* mRNA in *loft* siblings and mutants. (A-B) Bright-field view showed the plicated tail fin in *loft* mutants (54/209, ~25.5% mutants) (B) compared to siblings (A) from heterozygous *loft* mutant crossing at 3 dpf. (C-F) Whole-mount *in situ* hybridization analysis showed that either *slc39a1* (C, D) or *strc* mRNA (E, F) expression was unaffected in *loft* mutants (D, F) compared to siblings (C, E) at 3 dpa. Scale bars, 200 μ m.

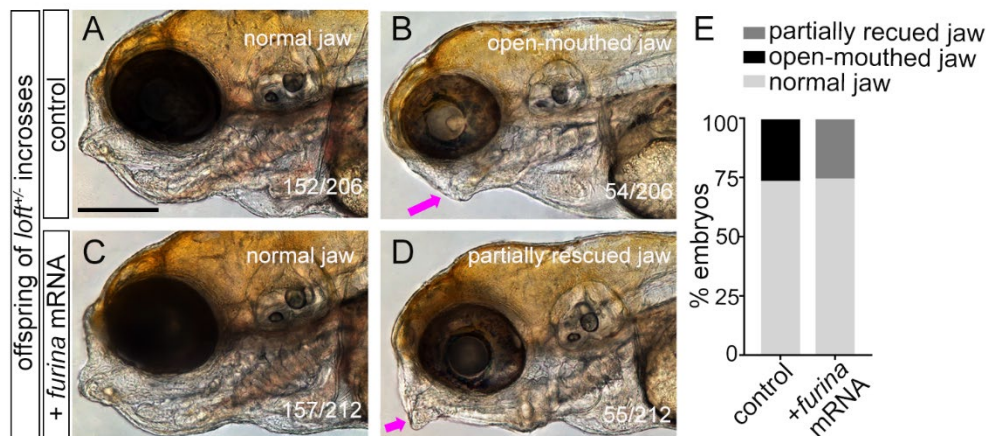


Fig. S2. *furina* mRNA injection rescues jaw defects in *loft* mutants. Control embryos from heterozygous *loft* mutant crossing resulted in 74% normal jaw embryos (A, 152/206) and 26% abnormal open-mouthed jaw embryos (B, 54/206), while *furina* mRNA injected embryos had 74% normal jaw (C, 157/212) and 26% partially rescued jaw (D, 55/212). (E) Bar graph showing panels A-D data. Magenta arrows point to the zebrafish jaw. Scale bars: 200 μ m.

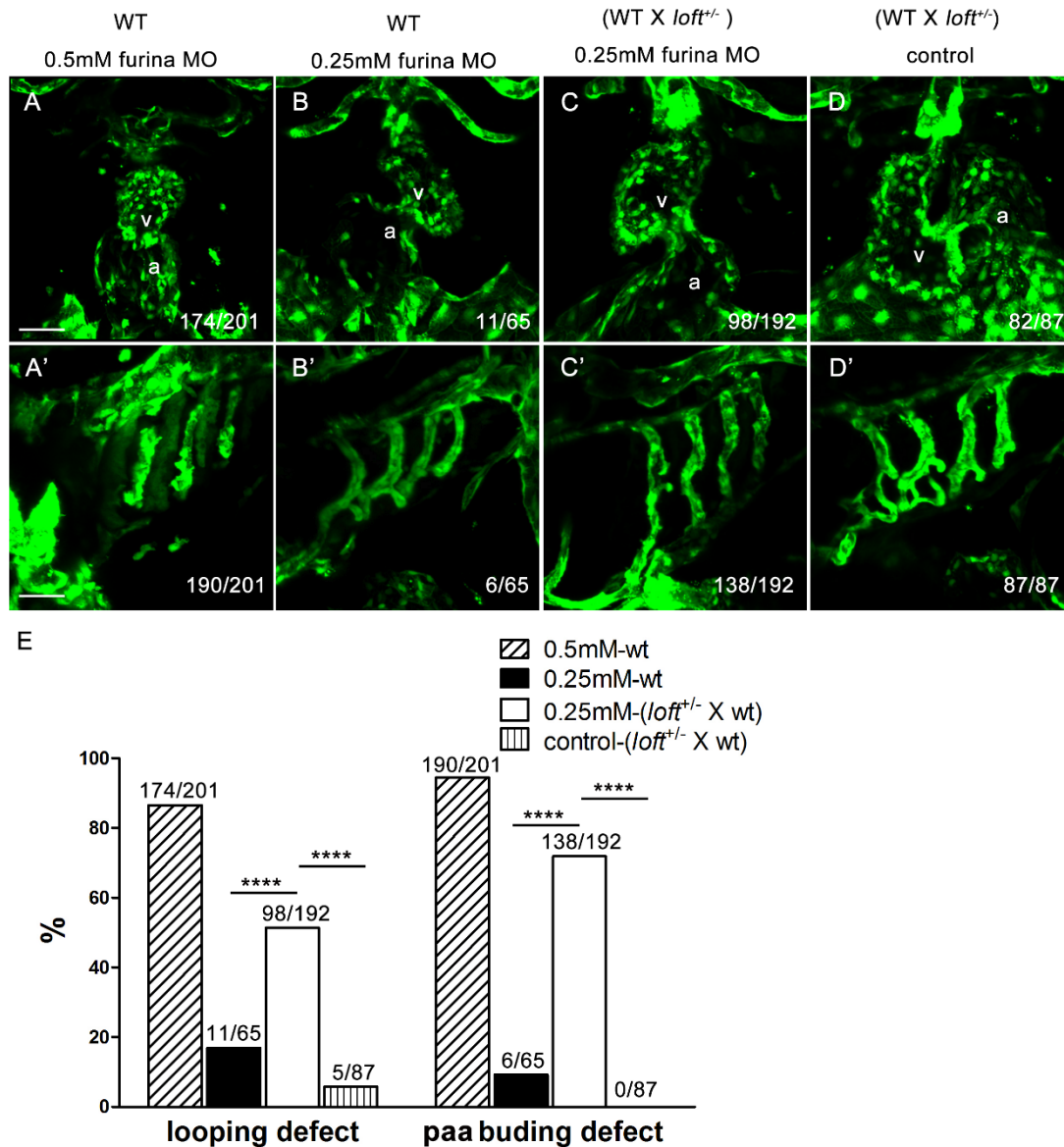


Fig. S3. *furina* MO knockdown causes defects in both pharyngeal arch artery and heart looping in zebrafish. (A, A') Wild-type embryos injected with 0.5 mM *furina* MO had severe defects of both heart looping (A) and pharyngeal arch artery (A'). *Tg(kdrl:GFP)* was used to label blood vessels and the endocardium. (B, B') WT embryos injected with 0.25 mM *furina* MO had fewer embryos with abnormal heart looping and pharyngeal arch artery. (C, C') More than half of embryos that were heterozygous *loft* mutants sensitized to 0.25 mM *furina* MO, resulting in defects of both heart looping (C; 98/192) and pharyngeal arch artery (C'; 138/192). Either WT or heterozygous *loft* mutants had little defects in heart looping and pharyngeal arch artery (D, D'). (E) Statistics showing the effects of *furina* MO from the above experiments (A-D; A'-D'). ****p<0.0001, chi-squared test. v, ventricle; a, atrium; scale bars: 30 μ m (A-D; A'-D').

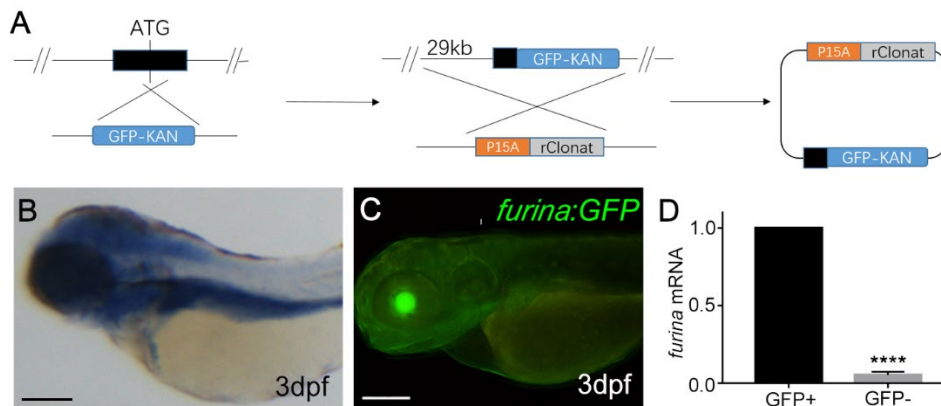


Fig. S4. The *TgBAC(furina:GFP)* fluorescent signals mimics endogenous *furina* expression. (A) Construction of *furina:GFP* reporter. As described in Materials and Methods, the *furina* gene-containing BAC, CH211-194N16, was transfected into DY380 to aid the insertion of the GFP-KAN fragment at 500 nucleotides downstream from the *furina* ATG by DNA homologous recombination; and about 30-kb BAC fragment was subcloned into the PNPC2 plasmid to form the *furina:GFP* construct that contains a 29-kb *furina* promoter and 1-kb GFP-KAN reporter flanked with I-Sce I sites on facilitating transgenesis in zebrafish. (B) *furina* mRNA *in situ* hybridization showed a broad expression pattern at 3 dpf. (C) The *TgBAC(furina:GFP)* reporter line also showed a broad GFP expression pattern at 3 dpf. (D) qRT-PCR analysis showed that *furina* mRNA expression was enriched in GFP-positive cells but barely detected in GFP-negative cells that were sorted from *TgBAC(furina:GFP)* transgenic embryos at 2 dpf. GAPDH was used to normalize mRNA. Statistical analysis was performed by unpaired two-tailed Student's t-test; **** $p < 0.0001$ (n=4). Scale bars, 200 μ m.

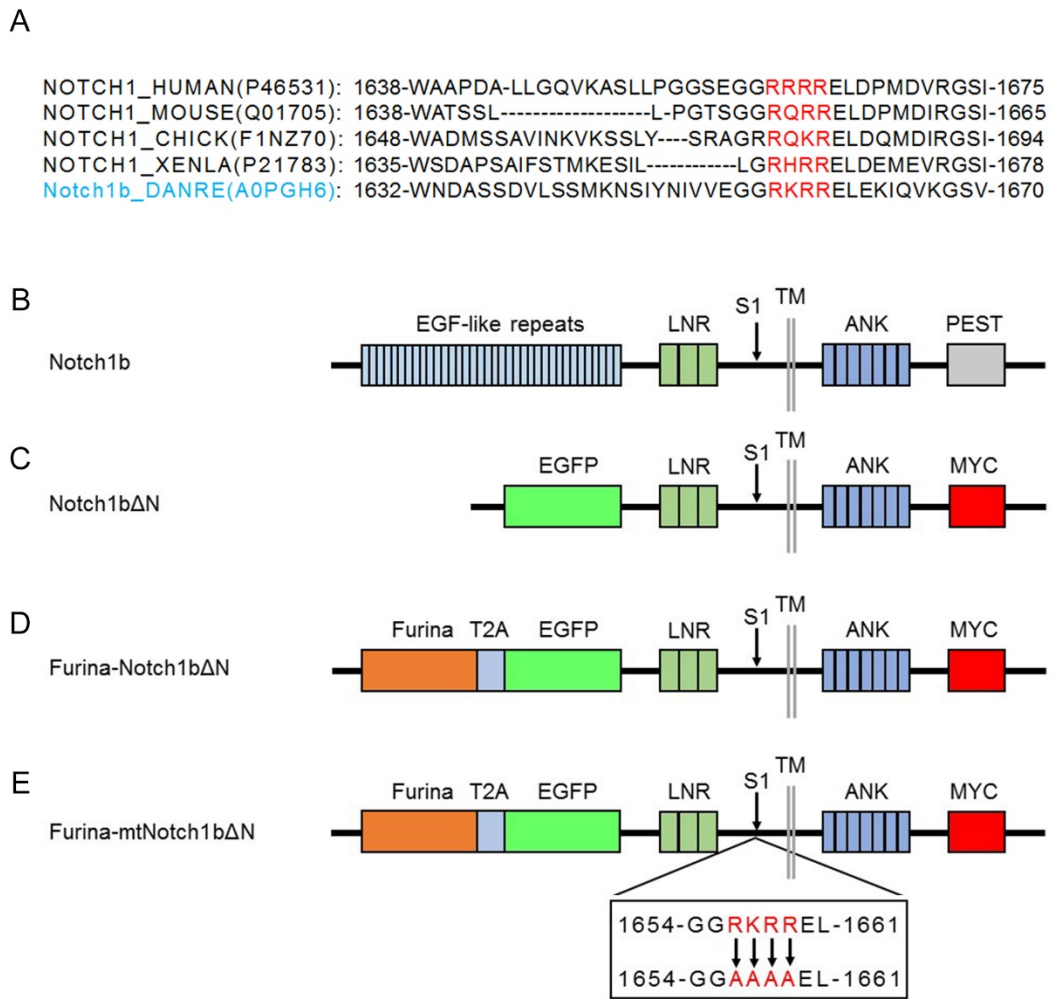


Fig. S5. Maps of expression constructs in zebrafish Notch1b and Notch1b mutant variants with Furin recognition sequences in Figure 6A. (A) Zebrafish Notch1b (blue) has a conserved 4-amino-acid Furin recognition sequence (red) by alignment with the human, mouse, chick, and *Xenopus laevis* Notch1b protein sequences. (B) Zebrafish Notch1b consists of EGF-like repeats, Lin-12-Notch repeats (LNR), Furin recognition/cleavage site (S1), transmembrane domain (TM), ankyrin repeats (ANK), and a proline, glutamate, serine, threonine-rich sequence (PEST). (C) Notch1bΔN consists of fusion of EGFP-Notch1b, in which the N-terminal EGF-like repeats of Notch1b are deleted. (D) Furina-Notch1bΔN consists of a fusion of Furina and Notch1bΔN by T2A peptide. (E) Furina-mtNotch1bΔN is a mutant variant of Furina-Notch1bΔN, in which the Furin cleavage-site amino-acids are mutated from RKRR to AAAA.

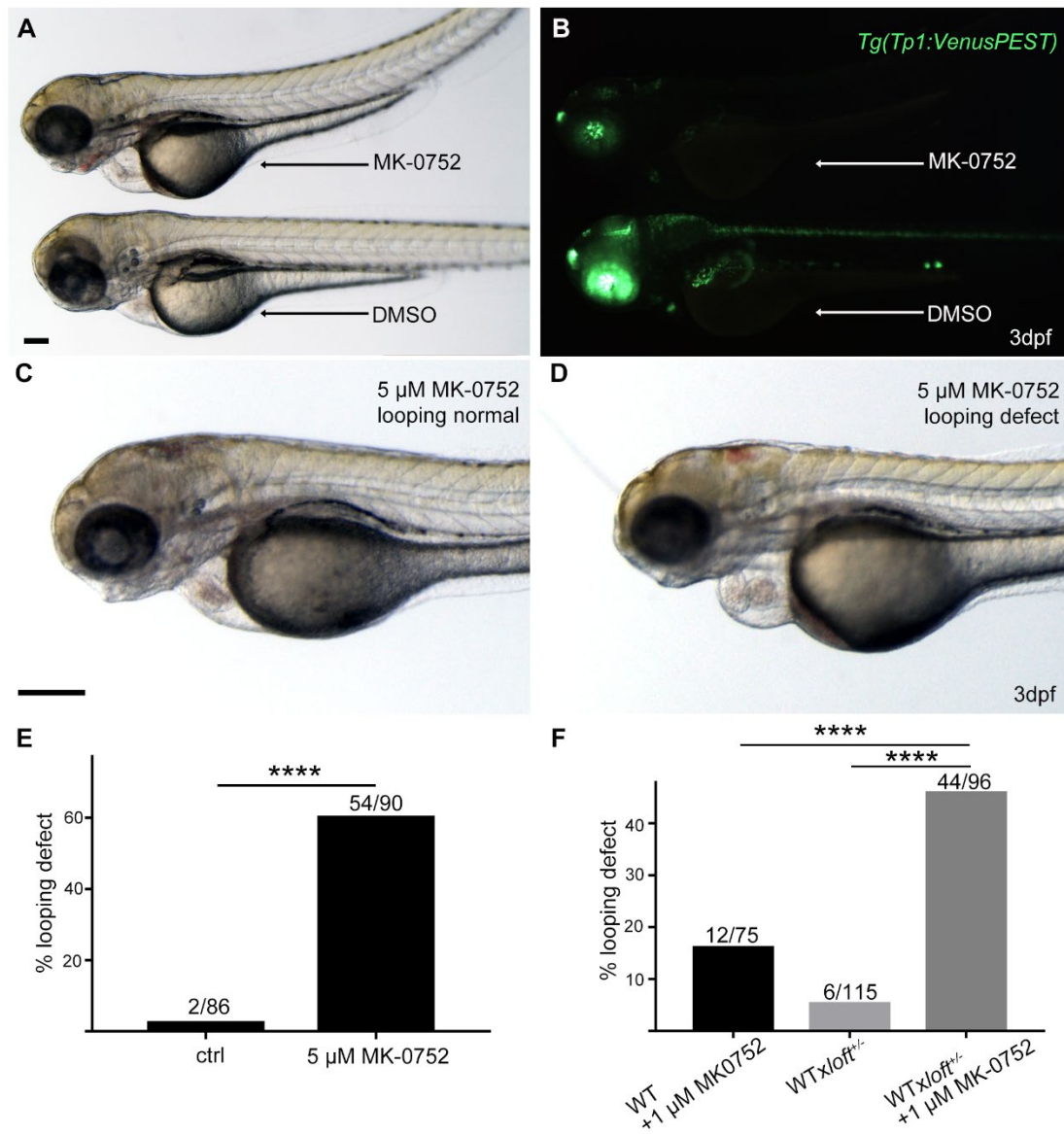


Fig. S6. Chemical inhibition of Notch signaling after cardiac jogging development causes cardiac looping defects. (A-B) *Tg(Tp1:Venus)* embryos at 24 hpf were selected and treated with 5 μM γ -secretase inhibitor MK-0752 or DMSO. At 3 dpf, DMSO-treated *Tg(Tp1:Venus)* embryos showed strong Venus expression (the lower embryo, 57/57), while MK-0752-treated embryos had decreased Venus signals (the upper embryo, 71/73). The same two embryos were photographed in bright field (A) or fluorescence (B). (C-D) Wild type embryos at 24 hpf were treated with 5 μM γ -secretase inhibitor MK-0752 and cardiac looping phenotype was scored at 3 dpa. (E) Statistics showing that embryos treated with 5 μM MK-0752 exhibited more looping defects compared to DMSO treated control group. **** $p < 0.0001$, chi-squared test. (F) Statistics showing that either wild-type embryos treated with 1 μM MK-0752 or heterozygous *loft* mutant embryos had fewer percentage of embryos with looping defects than heterozygous embryos treated with 1 μM MK-0752. Chi-squared test, **** $p < 0.0001$. Scale bars: 200 μm.

Table S1. The expression level of related genes from RNA-seq data.

Gene name	sib1-RPKM	sib2-RPKM	mt1-RPKM	mt2-RPKM
<i>furina</i>	75.045915	65.05494	0.162263	0.361089
<i>furinb</i>	0.5383708	0.133766	0.155751	0.236316
<i>slc39a1</i>	68.23331	62.74974	153.886	104.5721
<i>notch1a</i>	0.435532	0.322744	0.215526	0.523217
<i>notch1b</i>	35.329598	82.22417	63.43966	41.3028
<i>notch2</i>	3.163863	1.854625	2.490717	1.533975
<i>notch3</i>	0.5614235	0.590167	0.374816	0.265392
<i>strc</i>	0	0.127139	0	0

The expression level of partial genes that were mentioned in this work. The ventricles of *loft* mutants (mt1, mt2) and siblings (sib1, sib2) were isolated and subjected to transcriptome analysis. RPKM (Reads Per Kilobase of transcript, per Million mapped reads) was used to evaluate the mRNA expression level.

Table S2. Primer sequences of genetic markers in Figure 2.

Primer name	Sequence
z1206 F	CGTCTGACAGCCTGCATG
z1206 R	CTCGGCGCAGTAGGGAAC
syt7-16 F	GAGCACAACCAAGTCATACCC
syt7-16 R	GATCCAACCTGCAACCTCTCC
AF-10 F	CGAAGGAGATCCAGGAGTGA
AF-10 R	CTCCTGCATGTCTGTGGTGT
furina-7 F	AGACCCGCATAATCGTGTTTC
furina-7 R	TTAATAACGCACGGCAAATG
zgc112142-13 F	GCAACATTTCTCATGCCAGT
zgc112142-13 R	TGCAAGCGAATGTCTCTGAT
kirrela-4 F	TAGCAGACGAGCCAATACCC
kirrela-4 R	GGGTTCCCTACAACATGAGC
slc7a7-2 F	GCTCTTTATGATCGCCCTGT
slc7a7-2 R	TTGAGATCTTTAGGTGACATCTGG
z33744 F	TTCAAACACAAATCAGTGTCC
z33744 R	TACCAGCCTCCATTTATGGC

These genetic markers represent CA repeats markers for genetic linkage analysis, chromosomal walking, and genetic interval determination on the *loft* locus as shown in Figure 2.

Table S3. Primer sequences for generating *in situ* probes.

Primer name	Sequence
furina F	ATCGAAATTAACCCTCACTAAAGGGAACAAATGTG GGACCTCAGCATAAA
furina T7R	ATCGATAATACGACTCACTATAGGGAGAGCTCTTC TTGGCCTAAGTGCTGTT
notch1a F	TAATAATGTGGATGCTGCTGTCGT
notch1a T7R	TAATACGACTCACTATAGGGCAGACAAGTTGGAAT GTGGAGATG
notch1b F	GCAAGACGGAAAGGGAAACTTATT
notch1b T7R	TAATACGACTCACTATAGGGAATGTGCCTTCATTTA GCGAATC
notch2 F	AGATGGTTTCACTCCTCTCATGCT
notch2 T7R	TAATACGACTCACTATAGGGAATCCACAGGAGACA TGGTAAC
notch3 F	TCTCTGGTAGCCACACACTCTCAC
notch3 T7R	TAATACGACTCACTATAGGGCCTGAGATGGAATAG CTTGTGCTT
strc-F	CGACGAGCAACGTGAAGCAC
strc T7R	TAATACGACTCACTATAGGGATCTTTAAGATATTAG TCATGCCG

These forward and reverse primers were used to isolate *furina*, *notch1a*, *notch1b*, *notch2*, and *notch3* cDNA fragments by PCR of the first-strand cDNA of embryos from 2 to 3 dpf shown in Figures 2 and 5.

Table S4. Primer sequences for quantitative RT-PCR, BAC construct, *furina* mRNA synthesis, hsp70l:N1bICD-GFP construct, and Notch1bΔN construct.

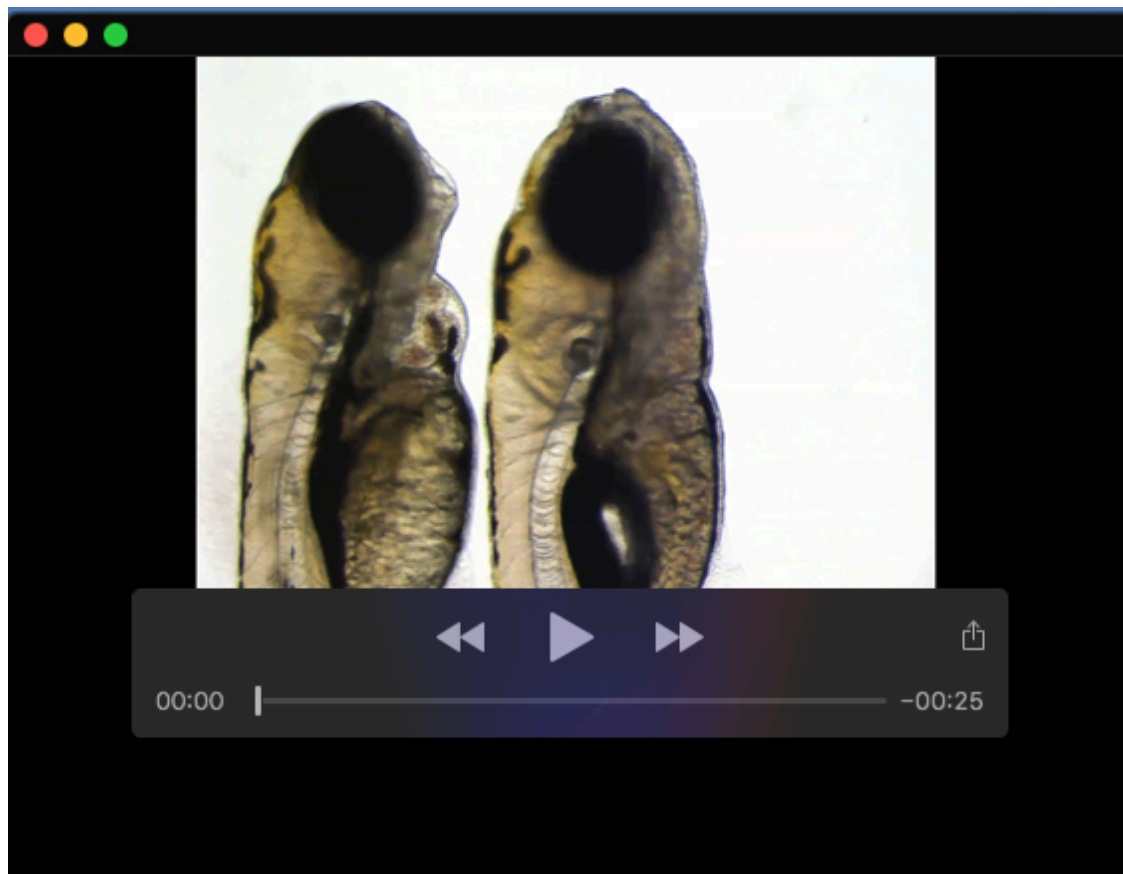
Primer name	Sequence
gapdh-F	GGTGGTGCAAAGAGAGTCATCATC
gapdh-R	ATCAACGGTCTTCTGTGTTGCTGT
Furina-F	TACTCCTCTGAGGGCTTCAATGAC
Furina-R	GCAGATCTGATTGAGGTCGTAGGT
	GACTTGGTGACATTAGGAATTCCTGCCTTGGTTCTCCTA
Furina GFP-F''	TAGTGTGGCCACCATGGTGAGCAAGGGCGAGGAGCTGT
	TC
	CTGAGCATACTGGCGTTACAAAGATGGCCACCGAGTGA
Furina KAN-R''	AATGACTTCCTGCCGCGTGTAGGCTGGAGCTGCTTC
Upstream furina 29-	GCAGCACTGCATGTTTTGGATGTCTTCTTTGCCTGTCAC
kb HA primer-F	ACCCAATACAGTAGGGATAACAGGGTAATTGCACTG
Downstream frt-	CCGCGTGTAGGCTGGAGCTGCTTCGACTAGTGGACCGA
KAN HA primer-R	AGTTCCTATACTCCGTAGGGATAACAGGGTAATTTAAG
furina-(mRNA)F	AAGCTGATGCTGTTGAGGTGATTC
furina-(mRNA)R	GGACTAGTCCAGTATTCAGACGAACCCCAGAAGG
hsp70l-N1bICD-F	AAACGGCGCCGGGAACAC
hsp70l-N1bICD-R	ACCGTTCATGACGTTTGAACCG
Notch1bΔN-F	TGCGAGATTGAGCAGTGTAAGTCAAG
Notch1bΔN-R	GGAATCCACCGGAGAGAGAACAGC

The primers (gapdh-F, gapdh-R, furina-F, and furin-R) were used to perform quantitative PCR shown in Figure 2; the primers (Furin GFP-F'', Furina KAN-R'', Upstream furina 29-kb HA primer-F, and Downstream fit-KAN HA primer R) were used to make *furina*:GFP reporter construct in Figure 4; the primers furin-(mRNA)F and furina-(mRNA)R were used to perform *in vitro* synthesis of *furina* mRNA in Figure 2; the primers (hsp70l-N1bICD-F and hsp70l-N1bICD-R) were used to make hsp70l:N1bICD-GFP construct in Figure 6; the primers (Notch1bΔN-F and Notch1bΔN-R) were used to make Notch1bΔN construct.

Table S5. The *furina* TALEN target.

Left arm	Cut site	Right arm
TATTATCACTTCAG	gcaccgcacggtgg	TGAAGAGGTCTTT

The target sequences showing that the left and right arm of TALEN sequences, as well as the restriction enzyme site sequences of the *furina* locus in Figure 3.



Movie 1. Time-lapse images showing the circulation of *loft* mutants and sibling embryos at 4 dpf. The *loft* mutant is on the left and control sibling embryo is on the right. Images were acquired at 100 frame/second for 32 seconds with a 10× air objective of Leica DM5000B microscopy.